Response to interactive comment on "Nitrate formation from heterogeneous uptake of dinitrogen pentoxide during a severe winter haze in southern China" by Hui Yun et al. from anonymous Referee #1

The reviewers' comments are italicized followed by our responses and changes in manuscript shown in blue and red, respectively. And the corrections are also marked as red color in the revised manuscript.

The manuscript of Yun et al., reported half month measurement of N_2O_5, $ClNO_2$ and other relative parameters during heavy haze episodes in Pearl River Delta (PRD) of southern China. The N_2O_5 uptake coefficient and $ClNO_2$ yield were determined from the observations. The study showed the observation evidence of the enhancement of particulate nitrate in the first several hours can be fully explained by the N_2O_5 heterogeneous hydrolysis and even comparable with the nitric acid formed by $OH+NO_2$ during daytime. Overall, the paper contributes to the knowledge of N_2O_5 heterogeneous chemistry and highlight the heterogeneous reactions in the formation of particulate nitrate in southern China. The following comments should be addressed before publishing on ACP.

Response: We appreciate the reviewer for the positive comments which are addressed in detail below.

Major comments:

The steady state assumption to derive the N_2O_5 uptake coefficient needs to be verified by model simulations under the observed conditions (with input from NO, NO_2, O_3, VOCs). It is useful to try other method (e.g. Brown et al., 2006) to derive N_2O_5 uptake coefficient.

Brown, S. S., Ryerson, T. B., Wollny, A. G., Brock, C. A., Peltier, R., Sullivan, A. P., Weber, R. J., Dube, W. P., Trainer, M., Meagher, J. F., Fehsenfeld, F. C., and Ravishankara, A. R.: Variability in nocturnal nitrogen oxide processing and its role in regional air quality, Science, 311, 67-70, DOI 10.1126/science.1120120, 2006.

Response: The method used to derive the N_2O_5 uptake coefficient in our manuscript did not require an assumption of NO_3 radical being in steady state, but assumed that the change of

NO$_3$ and N$_2$O$_5$ concentrations was mainly caused by NO$_3$/N$_2$O$_5$ chemistry. The value of $\frac{d([N_2O_5]+[NO_3])}{dt}$ was not required to be nearly zero as the method of Brown et al., 2006, but was calculated with the measured concentration of N$_2$O$_5$ and the calculated concentration of NO$_3$. We believe our method allows more data for use in analysis than the steady-state approach.

Indeed we compare our method with the steady-state approximation (Brown et al., 2006) for calculation of the γ_{N2O5} using equation (1) below. The plots of $\tau_{N2O5}{}^{-1}K_{eq}[NO_2]$ correlated to $0.25c_{N2O5}SaK_{eq}[NO_2]$ for four selected air masses in short-time periods which were proper to use the steady state assumption are presented in Figure 1 here. The $\gamma_{N2O5\text{-steady-state}}$ varied from 0.008 to 0.012 and was comparable to the uptake coefficients derived with the method in the manuscript in the same periods (see Table 1 here).

(1) $\tau_{N2O5}{}^{-1}K_{eq}[NO_2] \approx k_g + \frac{1}{4}C_{N2O5}\,Sa\,\gamma_{N2O5}K_{eq}[NO_2]$
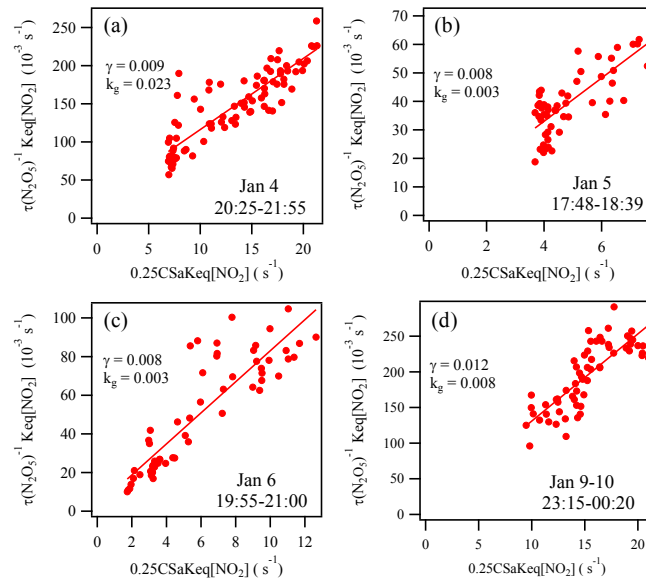
Figure 1. Plots of $\tau_{N2O5}{}^{-1}K_{eq}[NO_2]$ versus $0.25c_{N2O5}SaK_{eq}[NO_2]$ for selected air masses.

Table 1. Comparison of γ_{N2O5} derived with steady state method and with the method in the manuscript in the same periods.

Date	$\gamma_{N2O5\text{-steady-state}}$	$\gamma_{N2O5\text{-in the manuscript}}$
Jan 4 20:26-21:56	0.009	0.011
Jan 5 17:48-18:39	0.008	0.007
Jan 6 19:55-21:00	0.008	0.009
Jan 9 23:15-00:20	0.012	0.014

Without the need for steady-state assumption, we can make use of more observation data to derive the updated parameters.

The uncertainty of the measured N$_2$O$_5$, NMHC and Sa and the overall uncertainty propagated to N$_2$O$_5$ uptake coefficient and ClNO$_2$ yield should be carefully evaluated and discussed. As the hygroscopic growth factor is hard to quantify for RH over 90%, the derived N$_2$O$_5$ uptake coefficient for those conditions may subject with larger uncertainties compared with other RH cases. This is an interesting point to be discussed.

Response: The uncertainty of the measured N$_2$O$_5$ and NMHC was ±25% and ±20%, respectively, which will influence the item of $\frac{k_{NO_2+O_3}[NO_2][O_3]}{[N_2O_5]}$ and $\frac{\sum k_i[VOC_i]}{[NO_2]\times K_{eq}}$ in equation (2) here. According to the calculation in our manuscript, k'$_{N2O5}$ was two orders of magnitude higher than that of $\frac{\sum k_i[VOC_i]}{[NO_2]\times K_{eq}}$, suggesting the value of $\frac{k_{NO_2+O_3}[NO_2][O_3]}{[N_2O_5]}$ was far more than $\frac{\sum k_i[VOC_i]}{[NO_2]\times K_{eq}}$. Hence, the uncertainty of N$_2$O$_5$ uptake coefficient was mainly caused by the uncertainty of N$_2$O$_5$, NO$_2$ (±20%), O$_3$ (±5%) and Sa. The hygroscopic growth factor is hard to quantify for RH over 90%, thus the calculated Sa would present large uncertainty when RH reached over 90%. The average RH ranged from 59-85% during the selected periods in Table 2 in the revised manuscript. The uncertainty of Sa with RH below 90% was estimated to be around ±30% (Tham et al., 2016;Wang Z et al., 2017). The uncertainty of the calculated N$_2$O$_5$ uptake coefficient was then derived to be ±45%. The uncertainty of ClNO$_2$ yield was mainly caused by the uncertainty of NO$_2$ (±20%), O$_3$ (±5%) and ClNO$_2$ (±25%) and was derived to be ±30%.

(2) $k'_{N_2O_5} = \dfrac{k_{NO_2+O_3}[NO_2][O_3]}{[N_2O_5]} - \dfrac{d[N_2O_5]}{[N_2O_5]dt} - \dfrac{d(\frac{[N_2O_5]}{[NO_2]\times K_{eq}})}{[N_2O_5]dt} - \dfrac{\sum k_i[VOC_i]}{[NO_2]\times K_{eq}} = \dfrac{1}{4}C_{N_2O_5}S_a\gamma_{N_2O_5}$

Tham, Y. J., Wang, Z., Li, Q., Yun, H., Wang, W., Wang, X., Xue, L., Lu, K., Ma, N., Bohn, B., Li, X., Kecorius, S., Größ, J., Shao, M., Wiedensohler, A., Zhang, Y., and Wang, T.: Significant concentrations of nitryl chloride sustained in the morning: investigations of the causes and impacts on ozone production in a polluted region of northern China, Atmos. Chem. Phys., 16, 14959-14977, 10.5194/acp-16-14959-2016, 2016.

Wang, Z., Wang, W., Tham, Y. J., Li, Q., Wang, H., Wen, L., Wang, X., and Wang, T.: Fast heterogeneous N_2O_5 uptake and $ClNO_2$ production in power plant and industrial plumes observed in the nocturnal residual layer over the North China Plain, Atmos. Chem. Phys., 17, 12361-12378, 10.5194/acp-17-12361-2017, 2017.

In the manuscript, the following sentences were added:

Line 338-341: The uncertainty of the above γ_{N2O5} was estimated to be ±45% due to the measurement uncertainty of N_2O_5 (±25%), NO_2 (±20%), O_3 (±5%) and Sa (±30%). The uncertainty of ϕ_{ClNO2} was mainly caused by the uncertainty of NO_2 (±20%), O_3 (±5%) and $ClNO_2$ (±25%) and was estimated to be ±30%.

The relationship between N_2O_5 uptake coefficient, $ClNO_2$ yield and the chemical properties of particles or the meteorological data (such as RH) should be investigated, especially in the part of text around Line 572 (table 1), the reason of the high gamma value in the Jan.3 17:40-20:50 should be addressed as which was much higher than other derived value.

Response: We examined the correlation between N_2O_5 uptake coefficient, $ClNO_2$ yield and the concentrations of aerosol compositions or RH, and the results did not show any significant dependence of uptake coefficient/yield on these parameters. The below Table was added in the SI as Table S2.

Table 2. Average values ($\mu g\ m^{-3}$) of $PM_{2.5}$ loadings and the composition of $PM_{2.5}$ during the time periods corresponding to Table 2 in the revised manuscript.

Date	Cl^-	NO_3^-	SO_4^{2-}	NH_4^+	OM	EC	$PM_{2.5}$
Jan.3 17:40-19:00	0.9	19.7	8.8	6.5	37.4	8.0	86.4
Jan 4 17:00-22:00	1.5	44.3	8.7	12.0	44.6	13.2	150.7
Jan 5 17:00-22:00	1.6	68.9	15.5	15.3	56.6	14.2	216.6
Jan 6 17:00-22:40	2.7	40.0	15.7	13.8	54.6	10.5	174.3
Jan 9 19:00-00:20	0.8	29.9	7.2	8.9	36.7	11.6	117.3

Regarding the Jan 3rd case, the concentration of N_2O_5 and the Sa were both the lowest in the five cases, and the P_{NO3} was the highest among all cases, leading to high N_2O_5 uptake coefficient. Taking a closer look at the data of that night, it can be divided into two periods with relatively high N_2O_5 of 200 pptv on average from 17:40-19:00 and low N_2O_5 of only 15 pptv on average from 19:10-20:50 (see Table 2 below and Figure 2 data in the red box). The second period was influenced more by fresh emission during the transportation of the air mass as indicated by the more variable NO_2 and O_3, making the calculation of γ_{N2O5} and ϕ_{ClNO2} more difficult. In the revised manuscript, we decided to drop the second period, and the γ_{N2O5} was 0.066 (17:40-19:00) in the Jan 3 case.

Table 3. Details for the two parts of the selected period from 17:40-20:50 on the night of Jan 3, 2017.

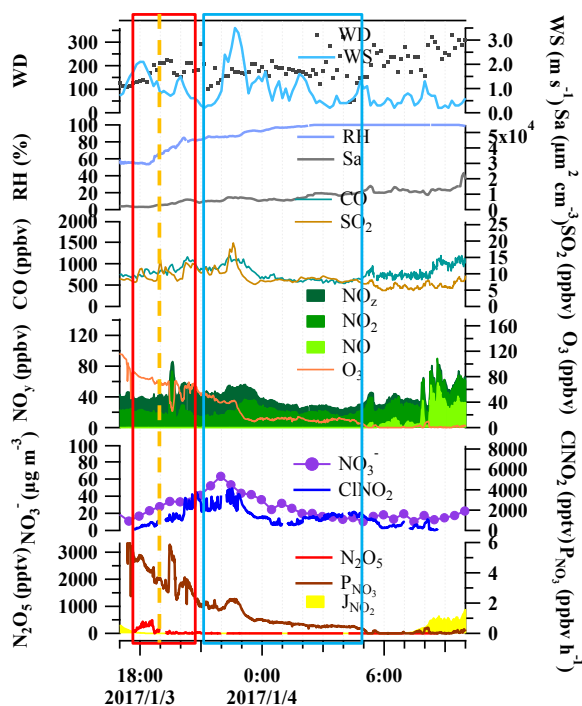| Date	N_2O_5 pptv	Max-$ClNO_2$ pptv	NO_2 ppbv	O_3 ppbv	RH %	Sa $\mu m^2\ cm^{-3}$	P_{NO3} ppbv h^{-1}	k_{NO3} $10^{-3}\ s^{-1}$	L_{N2O5} ppbv h^{-1}	$k_{NO3}/(Keq[NO_2])$ $10^{-5}\ s^{-1}$	k_{N2O5} $10^{-3}\ s^{-1}$	γ_{N2O5}	ϕ_{ClNO2}
Jan.3 17:40-19:00	200	1029	20.0	77.8	59	2170	4.3	0.516	4.3	3.03	8.8	0.066	0.18
Jan 3 19:10-20:50	15	3145	24.7	59.2	78	4970	3.5	0.840	3.5	3.68	41.2	0.162	0.36

Figure 2. Variation of N_2O_5, $ClNO_2$, NO_3^-, trace gases and meteorological conditions during the nighttime of Jan 3 to 4, 2017.

The related texts in the original manuscript were also revised carefully. The following sentences were added.

Line 327: The data show that the uptake coefficient ranged from 0.009 to 0.066.

Line 331-335: It is interesting to see much higher γ_{N2O5} (0.066) on Jan 3 than those in other four nights (0.009-0.015), resulting from higher P_{NO3} but much lower Sa and relatively low N_2O_5 concentrations on Jan 3. We examined known factors affecting the loss of NO_3 and N_2O_5 such as the concentrations of NO, NMHCs and aerosol compositions, but found no obvious difference between Jan 3 and other nights.

Line 341-343: The correlation between γ_{N2O5}, ϕ_{ClNO2} and the concentrations of aerosol compositions (see Table S2) or RH was investigated, and the results (not shown here) did not indicate any significant dependence of γ_{N2O5} or ϕ_{ClNO2} on these parameters.

Minor comments:

The description of the experimental setup of the key relevant parameters needs to be

strengthened, e.g. the limit of detection, the measurement uncertainties and measurement principle should be described.

Response: Table 1 with the limit of detection, the measurement uncertainties and measurement principle was added in the manuscript.

Table 1. Technique, limit of detection, and uncertainty of measuring instruments for trace gases and aerosols.

Species	Measurement techniques	Uncertainty	Detection limits
$ClNO_2$, N_2O_5	CIMS	±25%	6 pptv
HONO	LOPAP	±20%	7 pptv
O_3	UV photometry	±5%	0.5 ppbv
NO	Chemiluminescence	±20%	0.06 ppbv
NO_2	Photolytical converter & Chemiluminescence	±20%	0.3 ppbv
NO_y	MoO catalytic converter & Chemiluminescence	±5%	<0.1 ppbv
SO_2	Pulsed-UV fluorescence	±5%	0.1 ppbv
CO	IR photometry	±5%	4 ppbv
NMHCs	GC-FID/MS	±15-20%	20-300 pptv
OVOCs	DNPH-HPLC	±1-15%	20-450 pptv
$PM_{2.5}$	MAAP	±10%	<0.1 $\mu g\ m^{-3}$
Aerosol Ions	GAC-IC	±10%	0.01-0.16 $\mu g\ m^{-3}$
OC/EC	RT-4 SUNSET	± 4-6%	0.2 $\mu g\ cm^{-2}$

Line 161. The reference of Yue et al., 2015 may not appropriate and suggests replacing by Dong et al., 2012 Dong, H. B., Zeng, L. M., Hu, M., Wu, Y. S., Zhang, Y. H., Slanina, J., Zheng, M., Wang, Z. F., and Jansen, R.: Technical Note: The application of an improved gas and aerosol collector for ambient air pollutants in China, Atmos Chem Phys, 12, 10519-10533, 10.5194/acp-12-10519-2012, 2012.

Response: The suggested reference was adopted.

Line 586 (figure 2) please check the data of wind speed, as the WS keep below 3 m s^{-1} during the whole half month. And the plot style of NO$_y$ made the concentration of NO$_2$ hard to follow. The left y-axis of fourth panel should change to PM$_{2.5}$ or other more appropriate name.

Response: We did not find problem with the wind speed data, and the wind speed data shown in the figure was 10 min average. The very low wind speeds in the observation period were consistent with the regional meteorological conditions presented in the pressure contour in the weather chart. We also investigated the regional wind speed in PRD during this period from some websites and found that low wind speed was a regional phenomenon. Our personnel on site in fact felt little wind flow during the period. The figure below shows the wind speed (5 min average) from Dec 23, 2016 to Jan 20, 2017 at Heshan site, and the wind speed reached 7 m s^{-1} before Jan 2017. Therefore, the low wind speeds were real and conducive to the occurrence of the severe haze.
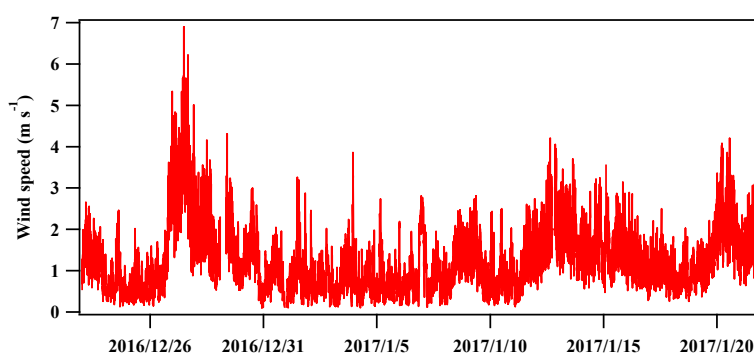

Figure 3. Wind speed from Dec 23, 2016 to Jan 20, 2017 at Heshan site.

The plot style of NO$_y$, NO$_2$ and NO was changed in the mentioned Figure. The left y-axis of fourth panel was changed to PM$_{2.5}$.

The legend of the early night and later night in figure 6 and 7 should be explained. By the way, how about the NO$_3^-$ formation potential intercomparison in the day and night of Jan 9 to 10.

Response: The periods in the early nighttime in Fig.6 and Fig.7 correspond to the periods in Table 2 in the revised manuscript. And the periods in the later nighttime correspond to the periods in Table 3 in the revised manuscript. So the captions of Fig.6 and Fig.7 were changed to make them better understood. The comparison of the NO$_3^-$ formation potential in the day and night of Jan 9 and 10 was not conducted due to the lack of data of NMHC after Jan 8 which made the model simulation of OH infeasible on the day of Jan 9. In the caption of Fig.7, the explanation was added as follows.

Line 680-684: Figure 6. Comparison between the measured NO_3^- increase and the NO_3^- formation potential in the early nighttime (periods in Table 2: Jan 3 17:40-19:00, Jan 4 17:00-22:00, Jan 5 17:00-22:00, Jan 6 17:00-22:40, Jan 9 19:00-00:20) and in the later nighttime (periods in Table 3: Jan 3-4 21:00-05:00, Jan 5 01:30-06:50, Jan 5-6 23:40-01:10, Jan 6-7 23:00-06:00, Jan 10 01:50-03:30).

Line 686-694: Figure 7. Comparison between the daytime (7:00 to 17:00 LT, assuming all gas phase HNO_3 partitioned into particle phase) and nighttime (17:00 to 7:00 LT of the next day) NO_3^- formation potential. The early nighttime in each day represents the periods in Table 2, including Jan 3 17:40-19:00, Jan 4 17:00-22:00, Jan 5 17:00-22:00, Jan 6 17:00-22:40, and Jan 9 19:00-00:20. The later nighttime in each day represents the periods in Table 3, including Jan 3-4 21:00-05:00, Jan 5 01:30-06:50, Jan 5-6 23:40-01:10, Jan 6-7 23:00-06:00, and Jan 10 01:50-03:30. The intercomparison of the NO_3^- formation potential in the day and night of Jan 9 and 10 was not conducted due to the lack of data of NMHC after Jan 8 which made the model simulation of OH infeasible on the day of Jan 9.

Response to interactive comment on "Nitrate formation from heterogeneous uptake of dinitrogen pentoxide during a severe winter haze in southern China" by Hui Yun et al. from Anonymous Referee #2

The reviewers' comments are italicized followed by our responses and changes in manuscript shown in blue and red, respectively. And the corrections are also marked as red color in the revised manuscript.

Yun et al. present a suite of measurements related N_2O_5 formation and subsequent uptake to aerosol that take place in a semi-rural area of China. They show through interpretations of their measurements and some master chemical modeling that nocturnal NO_x chemistry can likely account nearly 50% of aerosol nitrate mass loadings during these heavy pollution events.

This paper is written and presented well for the most part. The measurement methods portion is lacking even considering that an associated reference may describe additional details. Assuming my comments are appropriately addressed and some changes are made that would help to clarify the methods and the paper in general, I would recommend publication.

Response: We appreciate the reviewer for the positive comments and helpful suggestions. The measurement method portion was rewritten and a table was added to present the detection limit and uncertainties for CIMS and other related instruments. More references were cited for details of the instruments.

Table 1. Technique, limit of detection, and uncertainty of measuring instruments for trace gases and aerosols.

Species	Measurement techniques	Uncertainty	Detection limits
$ClNO_2$, N_2O_5	CIMS	±25%	6 pptv
HONO	LOPAP	±20%	7 pptv
O_3	UV photometry	±5%	0.5 ppbv
NO	Chemiluminescence	±20%	0.06 ppbv
NO_2	Photolytical converter & Chemiluminescence	±20%	0.3 ppbv
NO_y	MoO catalytic converter & Chemiluminescence	±5%	<0.1 ppbv
SO_2	Pulsed-UV fluorescence	±5%	0.1 ppbv
CO	IR photometry	±5%	4 ppbv
NMHCs	GC-FID/MS	±15-20%	20-300 pptv
OVOCs	DNPH-HPLC	±1–15%	20-450 pptv
$PM_{2.5}$	MAAP	±10%	<0.1 $\mu g\ m^{-3}$
Aerosol Ions	GAC-IC	±10%	0.01-0.16 $\mu g\ m^{-3}$
OC/EC	RT-4 SUNSET	± 4-6%	0.2 $\mu g\ cm^{-2}$

Comments:

Line 97: recommend changing "highest ever reported value" to something that will age better like "largest reported value to date".

Response: Adopted.

Line 100: recommend changing "aerosol formation" to "aerosol nitrate formation"

Response: Adopted.

Line 128: the SI would be a great place to see the results of these instrument backgrounds and the extent to which they worked.

Response: We added the relevant information on CIMS.

Line 127-129: Activated carbon packed in a filter was used to determine the instrument background which was 10.2 ± 2.2 and 8.9 ± 2.0 Hz on average for N_2O_5 and $ClNO_2$,

respectively.

Line 129: "standard gas of N_2O_5" sounds like you can purchase a standard cylinder of N_2O_5 (which you can't). Even if Wang et al. 2016 outlines these calibrations in more detail, a brief explanation is needed at the minimum. The description of these calibrations needs to be expanded and include $ClNO_2$ calibrations as well.

Response: The part of "2.2 Chemical ionization mass spectrometer" in the manuscript was rewritten.

Line 129-134: In-situ offline calibration was carried out every day for N_2O_5 and every two days for $ClNO_2$ by mixing the respective synthetic standard into humidified zero air (with RH controlled at 60% in the present study). The N_2O_5 standard was generated by reacting excess NO_2 with O_3 and determined from the decrease of NO_2, and the $ClNO_2$ was synthesized by the uptake of a known concentration of N_2O_5 on a NaCl slurry (see Wang T et al., 2016 and Tham et al., 2016 for details).

Line 132-133: How were detection limits calculated? What signal-to-noise was used, etc.? I think the authors only mean the uncertainty is +/- 25% not the precision.

Response: The detection limit was 6 pptv for both N_2O_5 and $ClNO_2$. It is defined as the signal twice of noise for 1 min averaged data. The noise was the standard error of the 1-min background measurement. The uncertainty of the measurement was estimated to be ± 25 % for both N_2O_5 and $ClNO_2$ (Wang et al., 2016).

Wang, T., Tham, Y. J., Xue, L., Li, Q., Zha, Q., Wang, Z., Poon, S. C., Dubé, W. P., Blake, D. R., and Louie, P. K.: Observations of nitryl chloride and modeling its source and effect on ozone in the planetary boundary layer of southern China, J. Geophys. Res. Atmos., 121, 2476–2489, doi: 10.1002/2015JD024556, 2016.

Line 137-138: The detection limits of N_2O_5 and $ClNO_2$ were both 6 pptv (2 σ, 1 min-averaged data).

Line 150-151: The uncertainty of the measurement was estimated to be ± 25 % for both N_2O_5 and $ClNO_2$ (Wang T et al., 2016).

Line 169: Here and throughout the paper it's probably best to change "aerosol surface density" to "aerosol surface area density" for clarity's sake.

Response: Adopted.

Line 182: consider changing "calculate" to "estimate"

Response: Adopted.

Line 214: change "matters" to "matter"

Response: Adopted.

Line 265/284: k' is often used for a pseudo first order rate constant. Consider using that to help differentiate from other rate constants.

Response: Adopted.

Line 307/309: make pNO_3^- and $p(NO_3^-)$ consistent. Use one or the other. $p(NO_3^-)$ is used in the rest of the paper.

Response: $p(NO_3^-)$ was used in all places of the paper.

Line 313/320 and Figure 6: Do the authors have a firm definition of what is considered "early nighttime" vs "late nighttime"? What times correspond to each period? Are these the same as provided in Table 1?

Response: The periods in the early nighttime in Fig.6 and Fig.7 correspond to the periods in Table 2 in the revised manuscript. And the periods in the later nighttime correspond to the periods in Table 3 in the revised manuscript. The captions of Fig.6 and Fig.7 have been changed to make them better understood.

Line 680-684: Figure 6. Comparison between the measured NO_3^- increase and the NO_3^- formation potential in the early nighttime (periods in Table 2: Jan 3 17:40-19:00, Jan 4 17:00-22:00, Jan 5 17:00-22:00, Jan 6 17:00-22:40, Jan 9 19:00-00:20) and in the later nighttime (periods in Table 3: Jan 3-4 21:00-05:00, Jan 5 01:30-06:50, Jan 5-6 23:40-01:10, Jan 6-7 23:00-06:00, Jan 10 01:50-03:30).

Line 686-694: Figure 7. Comparison between the daytime (7:00 to 17:00 LT, assuming all gas phase HNO_3 partitioned into particle phase) and nighttime (17:00 to 7:00 LT of the next day) NO_3^- formation potential. The early nighttime in each day represents the periods in Table 2, including Jan 3 17:40-19:00, Jan 4 17:00-22:00, Jan 5 17:00-22:00, Jan 6 17:00-22:40, and Jan 9 19:00-00:20. The later nighttime in each day represents the periods in Table 3, including Jan 3-4 21:00-05:00, Jan 5 01:30-06:50, Jan 5-6 23:40-01:10, Jan 6-7 23:00-06:00, and Jan 10 01:50-03:30.

Line 343-345: please change "cm^{-3}" units to commonly used "$molec\ cm^{-3}$".

Response: Adopted.

Line 359: certainly this approach is relevant to areas outside of China as well? Suggest removing "China".

Response: Adopted.

Table 1: Addition average aerosol nitrate loadings and $PM_{2.5}$ loadings for these periods would very useful. Consider adding all aerosol data (sulfate, ammonium, OM, etc.).

Response: A table for the average $PM_{2.5}$ loadings and the average concentrations of the main compositions of $PM_{2.5}$ were added into SI. We investigated the correlation between N_2O_5 uptake coefficient, $ClNO_2$ yield and the concentrations of aerosol compositions, and the results did not show any significant dependence of uptake coefficient/yield on any parameters.

Table S2. Average values ($\mu g\ m^{-3}$) of $PM_{2.5}$ loadings and the composition of $PM_{2.5}$ during the time periods corresponding to Table 2 in the revised manuscript.

Date	Cl^-	NO_3^-	SO_4^{2-}	NH_4^+	OM	EC	$PM_{2.5}$
Jan 3 17:40-19:00	0.9	19.7	8.8	6.5	37.4	8.0	86.4
Jan 4 17:00-22:00	1.5	44.3	8.7	12.0	44.6	13.2	150.7
Jan 5 17:00-22:00	1.6	68.9	15.5	15.3	56.6	14.2	216.6
Jan 6 17:00-22:40	2.7	40.0	15.7	13.8	54.6	10.5	174.3
Jan 9 19:00-00:20	0.8	29.9	7.2	8.9	36.7	11.6	117.3

Figure 5: Why not include the other aerosol data in this figure? NO_3^- does not track with Sa, so what is driving up Sa? The other data should explain this.

Response: We examined the measured aerosol composition data. Similar to nitrate, sulfate and ammonium did not show large increase, while $PM_{2.5}$ levels increased, contributing to the increase in Sa_dry by about 30% (see figure 1 below). The 5-fold rise in Sa_wet was mainly due to the RH increase from ~90% to nearly 100% leading to a sharp increase in the growth factor. For the calculation of N_2O_5 uptake coefficient and $ClNO_2$ yield in the five select cases, the high Sa values under RH more than 90% were not included.
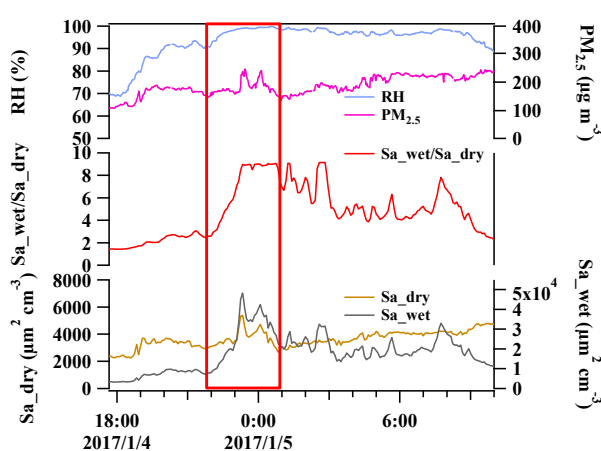

Figure 1. The variation of RH and $PM_{2.5}$ concentrations during the night of Jan 4-5 in the upper panel, the ratio of Sa_wet/Sa_dry in the middle panel, and Sa under dry conditions and the calculated Sa considering the variation of RH in the lower panel.

Have the authors considered boundary layer effects in any of their analyses? With a shallow nighttime inversion layer and little mixing many of these species could be further concentrated. Are there any measurements taken during the study that would give boundary layer information (sondes, etc.)?

Response: PBL was not measured at the site but should affect the variation of trace gas and aerosol concentration. We have added the following text in the revision.

Line 242-250: Apart from chemical reactions, the evolution of the Planetary Boundary Layer (PBL) also affects the concentrations of trace gas and aerosols. The height of PBL generally decreases after sunset with the faster drop in temperature of land, which could lead to the

accumulation of primary pollutants (and secondary pollutants) at surface if significant local sources are present. For example, on the night Jan 4-5 (see Fig 5), the CO and NO_y levels increased between 18:00-19:00 with enhancement of $ClNO_2$ and nitrate, indicative of accumulation of primary emissions, but afterward the primary pollutants decreased for three hours while the latter two continued to increase due to the nighttime chemical process.

Response to interactive comment on "Nitrate formation from heterogeneous uptake of dinitrogen pentoxide during a severe winter haze in southern China" by Hui Yun et al. from Anonymous Referee #3

The reviewers' comments are italicized followed by our responses and changes in manuscript shown in blue and red, respectively. And the corrections are also marked as red color in the revised manuscript.

The manuscript "Nitrate formation from heterogeneous uptake of dinitrogen pentoxide during a severe winter haze in southern China" by Yun and Co-authors uses observations of aerosol and gases and model results to study the contribution of heterogeneous chemistry via N_2O_5 to nitrate formation in $PM_{2.5}$ during severe winter haze episodes.

The measurements were carried out in the rural site of Heshan, located near the Perl River Delta in Southern China. In addition to a comprehensive suite of measurements, Yun and co-authors present the results of a chemical box model to estimate daytime HNO_3 mixing ratios. The box model was constrained by observation and its results were used to assess the importance of nighttime N_2O_5 over daytime HNO_3 as source of secondary aerosol nitrate.

The paper is well written, well structured and conveys results of interest for the scientific community. However, the method section (as pointed out by Refereees #1 and #2 as well) has to be improved and that some more discussion on 1)uncertainties, 2)sensitivity test of the model and 3)boundary layer dynamic needs to be added before publication.

Response: The description of the measurement method has been rewritten and some related references were added. A table presenting the detection limit and uncertainties for CIMS and other related instruments was added. Sensitivity tests were conducted by reducing 10% of the input concentrations of NMHCs to check the variation of the rate of $OH+NO_2$ during the daytime. We have added discussion on the role of boundary layer dynamics.

1) The description of the measurements should include the detection limits and the uncertainties, in particular for the species that were used to constrain the chemical box model.

Response: Table 1 with detection limits and measurement uncertainties was added in the revised manuscript.

Table 1. Technique, limit of detection, and uncertainty of measuring instruments for trace gases and aerosols.

Species	Measurement techniques	Uncertainty	Detection limits
$ClNO_2$, N_2O_5	CIMS	±25%	6 pptv
HONO	LOPAP	±20%	7 pptv
O_3	UV photometry	±5%	0.5 ppbv
NO	Chemiluminescence	±20%	0.06 ppbv
NO_2	Photolytical converter & Chemiluminescence	±20%	0.3 ppbv
NO_y	MoO catalytic converter & Chemiluminescence	±5%	<0.1 ppbv
SO_2	Pulsed-UV fluorescence	±5%	0.1 ppbv
CO	IR photometry	±5%	4 ppbv
NMHCs	GC-FID/MS	±15-20%	20-300 pptv
OVOCs	DNPH-HPLC	±1–15%	20-450 pptv
$PM_{2.5}$	MAAP	±10%	<0.1 $\mu g\ m^{-3}$
Aerosol Ions	GAC-IC	±10%	0.01-0.16 $\mu g\ m^{-3}$
OC/EC	RT-4 SUNSET	± 4-6%	0.2 $\mu g\ cm^{-2}$

2) There should be a discussion in the main text or in the SI about the sensitivity of the box model to the uncertainties of the measurements (this, for example should be communicated with uncertainty bars in figure 7).

Response: Sensitivity tests were carried out by reducing the input concentrations by 10% to check the deviation of the average daytime (7:00-17:00) rate of $OH+NO_2$ reaction. The method of Relative Increment Reactivity (RIR) was applied here as the index of the sensitivity (see the following equation). R_1 means the original rate of $OH+NO_2$ reaction, while $R_{0.9}$ means the rate of $OH+NO_2$ reaction after the input concentrations were reduced to 90%.

$$RIR=\frac{(R_1-R_{0.9})/R_1}{10\%}$$

NMHCs were categorized into four groups, including C4HC, LRHC, AROM and OLF, which

represent alkanes with $\geqslant 4$ carbons, hydrocarbons with low reactivity (including ethane, propane and benzene), reactive aromatics (including all aromatics except for benzene), and reactive olefins (including all alkenes), respectively (Xue et al., 2014). From the following figure, the simulated rate of $OH+NO_2$ reaction was most sensitive to HONO (RIR of 0.6-0.8), followed by NO_x (RIR of 0.2-0.5) and OVOCs (RIR of 0-0.2).
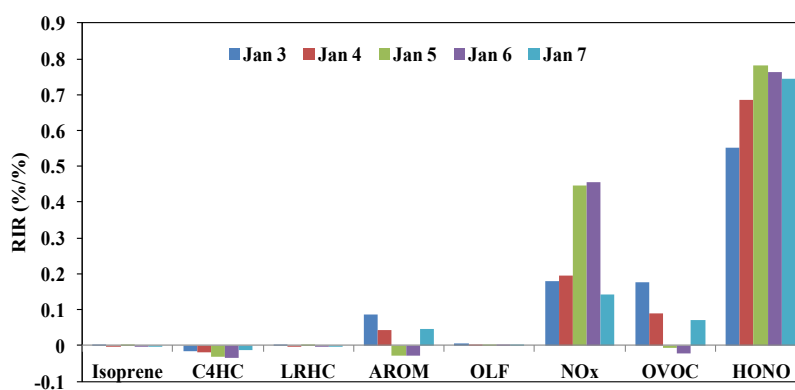

Figure 1. OBM-calculated RIRs to check the sensitivity of the average daytime (7:00-17:00) rate of $OH+NO_2$ reaction to the uncertainties of the measured input data.

Xue, L., Wang, T., Louie, P. K. K., Luk, C. W. Y., Blake, D. R., and Xu, Z.: Increasing external effects negate local efforts to control ozone air pollution: A case study of Hong Kong and implications for other chinese cities, Environmental Science and Technology, 48, 10769-10775, 10.1021/ es503278g, 2014.

Line 211-214: Sensitivity tests were carried out by reducing the input concentrations by 10% to check the deviation of the average daytime (7:00-17:00) rate of $OH+NO_2$ reaction. The simulated rate of $OH+NO_2$ reaction was most sensitive to HONO, followed by NO_x and OVOCs (see Text. S1 and Fig. S2).

3) In paragraph 2.2 a discussion about interference for species with the same nominal mass as $I(N_2O_5)^-$ and $I(ClNO_2)^-$ should be added. How much contribution from other species would Yun and Co-authors expect? If it was not negligible how would change the results from the box model/comparison?

Response: To the best of our knowledge, no interference was reported for $I(N_2O_5)^-$ at 235 m/z in current publications. Besides, we compared ambient measurements of N_2O_5 using the

quadrupole CIMS and NOAA-CRDS in 2016 (Wang et al., 2016), and N_2O_5 measured by CIMS and CRDS matched well with each other (slope=0.99, R^2=0.93). Recent ambient measurement of $ClNO_2$ in Beijing with a Tof-CIMS showed that $I(HNO_3)(H_2O)^-$ may cause ~10% interference of $ClNO_2$ at 208 m/z (Breton et al., 2018), but this kind of interference cannot be resolved by a quadrupole CIMS. For the quadrupole CIMS, we checked the correlation between the measured signal at 208 m/z ($I^{35}ClNO_2^-$) and at 210 m/z ($I^{37}ClNO_2^-$) during the present field campaign. The slope (0.317, $R^2 = 0.99$) was very close to the theoretical value of chlorine isotopic ratio of 0.32. Overall, we do not expect large (>10%) interference to $ClNO_2$, and no known interference is known to the N_2O_5 signal.

Breton, M. L., Hallquist, Å. M., Pathak, R. K., Simpson, D., Wang, Y., Johansson, J., Zheng, J., Yang, Y., Shang, D., and Wang, H.: Chlorine oxidation of VOCs at a semi-rural site in Beijing: significant chlorine liberation from $ClNO_2$ and subsequent gas-and particle-phase Cl–VOC production, Atmospheric Chemistry and Physics, 18, 13013-13030, 2018.

Wang, T., Tham, Y. J., Xue, L., Li, Q., Zha, Q., Wang, Z., Poon, S. C., Dubé, W. P., Blake, D. R., and Louie, P. K.: Observations of nitryl chloride and modeling its source and effect on ozone in the planetary boundary layer of southern China, J. Geophys. Res. Atmos., 121, 2476–2489, doi: 10.1002/2015JD024556, 2016.

4) Relative humidity (RH) is known to affect measurements carried out with I-CIMS. Was the inlet used in this study humidified? Was the RH controlled/monitored during zero measurements? How could the zero affect the box model results (e.g., over/under estimation of N_2O_5/$ClNO_2$)? What are the biases that the 6 m sampling line could generate in their results?

Response: Similar to our previous practice, the effect of RH on the sensitivity of N_2O_5 and $ClNO_2$ was measured by altering the RH in calibration during the present campaign (see below figure). The sensitivity of N_2O_5 and $ClNO_2$ in ambient measurement was corrected based on the RH monitored in real-time in the CIMS inlet.
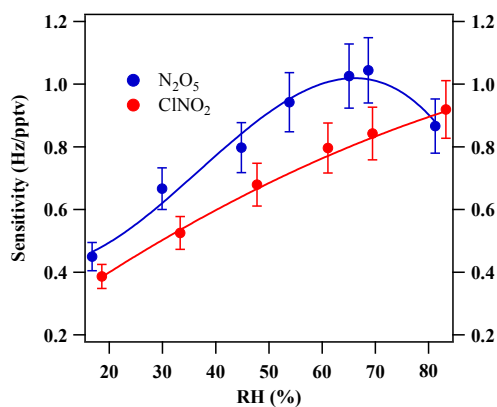
Figure 2. The sensitivity of CIMS as a function of RH for (a) N_2O_5 at 235 m/z and (b) $ClNO_2$ at 208 m/z at Heshan site.

The inlet in this study was not humidified. Since the sampling period in this study was humid enough (RH>40%) to form the reagent $I(H_2O)^-$, a humidified inlet was not necessary.

The RH was not controlled but monitored during zero (and ambient) measurements.

The zero signals were subtracted from the total signals during data processing, thus they do not affect final data and thus modeling results.

The 6 m sampling tubing was replaced every day in late afternoon. The wall loss of N_2O_5 was measured by injecting synthetic N_2O_5 each time before and after replacing the sampling tubing. The measured wall loss of N_2O_5 was ~10% for the clean tubing and increased to ~40% after one day's sampling. Because our analysis mainly focused on data in the first few hours of evening, the loss was insignificant and thus was not corrected in our final data. However, this bias can be important at later period before tube replacement.

In the revised manuscript, we have added description on dependence of sensitivity on RH and how to correct it and also the above figure as Fig. S1. We also added the following sentences.

Line 134-137: The average sensitivity of N_2O_5 and $ClNO_2$ was 0.9±0.3 and 0.7±0.2 Hz pptv^{-1}, respectively. The dependence of the sensitivity on the relative humidity was measured during the field study (see Fig. S1) which was used to correct for the RH effect based on the measured ambient RH values.

Line 145-150: The loss of N_2O_5 on the tubing wall was checked on site by injecting N_2O_5 into

the ambient air before and after the tubing replacement, and the loss was around 10% in the "clean" tubing and increased to nearly 40% in the next afternoon. Because our analysis mainly focused on data in the first few hours of evening, the loss was insignificant and thus was not corrected in our final data. However, this bias can be important at later period before tube replacement.

5) The boundary layer plays a significant role in the time evolution of the concentrations of nitrate in the particle. Yun and Co-authors make little to no mention of its role. For example, one might expect that particulate nitrate would increase also in the early morning hours due to the contribution of the residual layer during the mixing. This doesn't seem to happen in the observations presented in this work. May the Authors discuss why that would be the case?

Response: This point was also raised by other referees. The description of boundary layer dynamics has been added in the revised version. The absence of nitrate increase in the early morning in our study is consistent with previous observations at the site (Yue et al., 2015). It may be explained by enhanced evaporation of NH_4NO_3 to HNO_3 and NH_3 due to increased temperature.

Yue, D., Zhong, L., Zhang, T., Shen, J., Zhou, Y., Zeng, L., Dong, H., and Ye, S.: Pollution properties of water-soluble secondary inorganic ions in atmospheric $PM_{2.5}$ in the Pearl River Delta region, Aerosol Air Qual. Res, 15, 1737-1747, 2015.

6) An increase in particulate nitrate concentrations (as well as $PM_{2.5}$) could also be due to a dilution effect (same magnitude of aerosol sources but reduced volume in which the aerosols are mixed). I recommend adding a few sentences explaining how the mixing of the residual layer in the morning hours could affect the results presented here.

Response: The following discussion was added in the manuscript.

Line 242-250: Apart from chemical reactions, the evolution of the Planetary Boundary Layer (PBL) also affects the concentrations of trace gas and aerosols. The height of PBL generally decreases after sunset with the faster drop in temperature of land, which could lead to the accumulation of primary pollutants (and secondary pollutants) at surface if significant local sources are present. For example, on the night Jan 4-5 (see Fig 5), the CO and NO_y levels

increased between 18:00-19:00 with enhancement of $ClNO_2$ and nitrate, indicative of accumulation of primary emissions, but afterward the primary pollutants decreased for three hours while the latter two continued to increase due to the nighttime chemical process.

1 **Nitrate formation from heterogeneous uptake of dinitrogen pentoxide during a severe**

2 **winter haze in southern China**

3 Hui Yun[1], Weihao Wang[1], Tao Wang[1,*], Men Xia[1], Chuan Yu[1,2], Zhe Wang[1], Steven C.N.

4 Poon[1], Dingli Yue[3], Yan Zhou[3]

5 [1]Department of Civil and Environmental Engineering, The Hong Kong Polytechnic University,

6 Hong Kong, China

7 [2]Environment Research Institute, Shandong University, Jinan, China

8 [3]Guangdong Environmental Monitoring Center, State Environmental Protection Key

9 Laboratory of Regional Air Quality Monitoring, Guangzhou, China

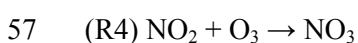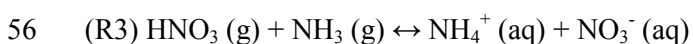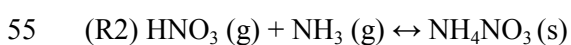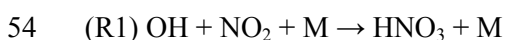10 *Correspondence to: Tao Wang (cetwang@polyu.edu.hk)*

11 **Abstract:** Nitrate (NO_3^-) has become a major component of fine particulate matter ($PM_{2.5}$)

12 during hazy days in China. However, the role of the heterogeneous reactions of dinitrogen

13 pentoxide (N_2O_5) in nitrate formation is not well constrained. In January 2017, a severe haze

14 event occurred in the Pearl River Delta (PRD) of southern China during which high levels of

15 $PM_{2.5}$ (~400 μg m^{-3}) and O_3 (~160 ppbv) were observed at a semi-rural site (Heshan) in the

16 western PRD. Nitrate concentrations were up to 108 μg m^{-3} (1 h time resolution), and the

17 contribution of nitrate to $PM_{2.5}$ reached nearly 40%. Concurrent increases in NO_3^- and $ClNO_2$

18 (with a maximum value of 8.3 ppbv in 1 min time resolution) were observed in the first

19 several hours after sunset, indicating an intense N_2O_5 heterogeneous uptake on aerosols. The

20 formation potential of NO_3^- via N_2O_5 heterogeneous reactions was estimated to be 29.0 to 77.3

21 μg m^{-3} in the early hours (2 to 6 h) after sunset based on the measurement data, which could

22 completely explain the measured increase in the NO_3^- concentration during the same time

23 period. Daytime production of nitric acid from the gas-phase reaction of OH + NO_2 was

24 calculated with a chemical box model built using the Master Chemical Mechanism (MCM

25 v3.3.1) and constrained by the measurement data. The integrated nocturnal nitrate formed via

26 N_2O_5 chemistry was comparable to or even higher than the nitric acid formed during the

27 daytime. This study confirms that N_2O_5 heterogeneous chemistry was a significant source of

28 aerosol nitrate during hazy days in southern China.

29 **Keywords:** N_2O_5, $ClNO_2$, nitrate, Pearl River Delta, southern China

1 Introduction

Severe haze in China has been a major concern of the regulatory and scientific communities in recent years. Nitrate was identified as an important component of $PM_{2.5}$ during hazy days in both summer and winter (e.g., Huang et al., 2014; Li et al., 2018; Pathak et al., 2009; Zhang et al., 2015). Moreover, the proportion of nitrate in $PM_{2.5}$ has increased steadily in the last decade due to the lagged control of NO_x emissions compared to SO_2 (Fu et al., 2014; Geng et al., 2017; Qu et al., 2017; Reuter et al., 2014; Wang X et al., 2016). As a result, the concentrations of nitrate in $PM_{2.5}/PM_{1.0}$ were even higher than those of sulfate during some haze events (Ge et al., 2017; Li et al., 2017; Liu et al., 2015; Yang et al., 2017; Yue et al., 2015).

Nitrate is formed from NO_x in both the daytime and nighttime. During the day, nitric acid (HNO_3) is produced through the gas-phase reaction between OH and NO_2 (R1), and this pathway is insignificant at night due to very low OH concentrations (e.g., Seinfeld and Pandis, 2016). The nitric acid can react with ammonia (NH_3) to form ammonium nitrate (NH_4NO_3), and an equilibrium can be reached for these three compounds between the gas phase and the particle phase (R2-3). In the nighttime, heterogeneous uptake of N_2O_5, which is formed from the reactions involving O_3, NO_2 and NO_3, becomes a source of nitrate and also produces gaseous $ClNO_2$ when chloride-containing aerosol is present (R4-7) (Finlayson-Pitts et al., 1989). This nitrate formation pathway is important only at night due to the fast photolysis of NO_3 during the day. Compared to the relatively well-understood formation of aerosol nitrate via the OH + NO_2 reaction, the contribution from N_2O_5 heterogeneous reactions has been poorly quantified due to the limited knowledge of key factors controlling the heterogeneous processes, such as the N_2O_5 uptake coefficient (γ_{N2O5}) and $ClNO_2$ yield (ϕ_{ClNO2}) (Brown and Stutz, 2012; Chang et al., 2011).

(R1) $OH + NO_2 + M \rightarrow HNO_3 + M$

(R2) $HNO_3 (g) + NH_3 (g) \leftrightarrow NH_4NO_3 (s)$

(R3) $HNO_3 (g) + NH_3 (g) \leftrightarrow NH_4^+ (aq) + NO_3^- (aq)$

(R4) $NO_2 + O_3 \rightarrow NO_3$

58   (R5) $NO_2 + NO_3 + M \leftrightarrow N_2O_5 + M$

59   (R6) $NO_3 + VOCs \rightarrow$ products

60   (R7) $N_2O_5 + H_2O$ or $Cl^- (aq) \rightarrow (2-\phi) NO_3^- (aq) + \phi ClNO_2 (g)$

61   Model studies initially treated γ_{N2O5} as a constant (0.03 to 0.1) (Dentener and Crutzen,

62   1993;Makar et al., 1998;Munger et al., 1998;Schaap et al., 2004;Wen et al., 2015;Xue et al.,

63   2014), and later utilized several parameterization schemes of γ_{N2O5} and ϕ_{ClNO2} based on the

64   laboratory investigations of their dependence on aerosol compositions and aerosol water

65   content (Anttila et al., 2006;Bertram and Thornton, 2009;Davis et al., 2008;Evans and Jacob,

66   2005;Riemer et al., 2009;Riemer et al., 2003;Roberts et al., 2009). However, recent studies

67   found a significant discrepancy between the field-derived and parameterized γ_{N2O5} and ϕ_{ClNO2}

68   (McDuffie et al., 2018; Phillips et al., 2016; Tham et al., 2018; Wang X et al., 2017; Wang Z

69   et al., 2017; Zhou et al., 2018). These findings suggest that N_2O_5 uptake is more complicated

70   than previously thought and a better understanding of the uptake process is needed to improve

71   the prediction of nitrate and haze.

72   In addition to the modeling approach, field measurements of trace gases and aerosol

73   composition have been used to infer the contribution of N_2O_5 heterogeneous chemistry to

74   nitrate formation. Pathak et al. (2009) postulated the importance of N_2O_5 heterogeneous

75   reactions to the high aerosol nitrate observed in summertime in Beijing and Shanghai by

76   examining the variation of nitrate with the change in relative humidity (RH) and the

77   equilibrium between anions and cations in $PM_{2.5}$. Pathak et al. (2011) further investigated

78   nitrate formation using a coupled aqueous phase radical mechanism (CAPRAM) and a

79   gas-phase chemistry mechanism (RACM, without $ClNO_2$ chemistry). By constraining the

80   uptake coefficient of N_2O_5 in the range of 0.001 to 0.1, they reproduced the observed

81   enhancement of nitrate and suggested that N_2O_5 uptake in aerosols contributed to 50 to 100%

82   of the nighttime increase in nitrate. A similar method was used recently by Wen et al. (2018)

83   to simulate the summertime nitrate formation in the North China Plain (NCP), which

84   demonstrated the dominant contribution of N_2O_5 heterogeneous reactions to nighttime nitrate

85   formation. Based on the observed covariation of nitrate and RH, Wang et al. (2009)

86   speculated that N_2O_5 reactions dominated the nitrate formation on polluted days with high

87   NO_2 and O_3 in Shanghai. Neither N_2O_5 nor $ClNO_2$ was measured during these early

88   observation-based studies. A recent study (Wang H et al., 2017) inferred γ_{N2O5} from the

89   measured N_2O_5 on four days in urban Beijing and estimated the lower limit of the formation

90   potential of aerosol nitrate assuming a unity ϕ_{ClNO2} because $ClNO_2$ was not measured. Their

91   result showed a comparable contribution to nitrate formation from the N_2O_5 heterogeneous

92   chemistry as from the daytime pathway of the $OH + NO_2$ reaction.

93   In the present study, N_2O_5, $ClNO_2$, the related chemical and meteorological parameters were

94   measured at a semi-rural site in the Pearl River Delta of southern China from Jan 2 to Jan 15,

95   2017. A severe haze event was observed during the field study with $PM_{2.5}$ reaching 400 μg m^{-3}

96   and O_3 up to 160 ppbv. $ClNO_2$, which is only known to be produced from N_2O_5 heterogeneous

97   uptake, reached up to 8.3 ppbv, which is the largest reported value to date and revealed

98   extremely active N_2O_5 chemistry during the episode. The concurrent measurements of N_2O_5,

99    $ClNO_2$ and aerosol nitrate provide better constraints for elucidating nighttime NO_3/N_2O_5

100   chemistry and aerosol nitrate formation. An overview of the measurement data was first

101   presented. The nighttime processes that led to the formation of nitrate (e.g., production of

102   NO_3 and N_2O_5, N_2O_5 uptake coefficient, $ClNO_2$ yield) were analyzed. The nighttime

103   formation potential of nitrate was estimated based on these data and compared to the

104   measured increase in nitrate. The daytime production of nitric acid via the $OH + NO_2$ reaction

105   was calculated based on a box model using the Master Chemical Mechanism (MCM v3.3.1)

106   and compared to the nighttime formation potential of nitrate.

107   **2 Methods**

108   **2.1 Site description**

109   The field observation was conducted at the Guangdong Atmospheric Supersite, a semi-rural

110   site located at Hua Guo Shan (HGS, 22.728°N, 112.929°E) in the southwest of the city of

111   Heshan from Jan 2 to Jan 15, 2017. As shown in Fig. 1, HGS is a hill with a height of 60 m

112   above sea level. All measurement instruments were located on the 4th floor of a four-story

113   building on the top of the hill. The observation site was located in the western PRD where the

114   economic activity and population density are much less compared to central PRD. There are

115   five main roads near the HGS site, including three national roads (G325, G94 and G15), and

116   two provincial roads (S272 and S270). The hill is covered by subtropical trees and surrounded

117   by similar hills within close range, and a few residents live at the foot of the hill with some

118   farmland in the area.

119   **2.2 Chemical ionization mass spectrometer**

120   N_2O_5 and $ClNO_2$ were simultaneously observed using a quadrupole chemical ionization mass

121   spectrometer (CIMS, THS Instruments, Atlanta). The same instrument had been used in

122   several previous studies in southern and northern China (Tham et al., 2016; Wang T et al.,

123   2016; Wang Z et al., 2017). The reader can refer to these earlier papers for detailed

124   description of the measurement principle, calibration, and maintenance procedures. Briefly,

125   ambient N_2O_5 and $ClNO_2$ are converted to ion clusters of $I(N_2O_5)^-$ and $I(ClNO_2)$ by Iodide

126   ions (I^-) produced by exposing CH_3I/N_2 (0.3%v/v) to an alpha radioactive source, 210-Po, and

127   are subsequently detected at 235 and 208 m/z, respectively. Activated carbon packed in a filter

128   was used to determine the instrument background which was 10.2 ± 2.2 and 8.9 ± 2.0 Hz on

129   average for N_2O_5 and $ClNO_2$, respectively. In-situ offline calibration was carried out every

130   day for N_2O_5 and every two days for $ClNO_2$ by mixing the respective synthetic standard into

131   humidified zero air (with RH controlled at 60% in the present study). The N_2O_5 standard was

132   generated by reacting excess NO_2 with O_3 and determined from the decrease of NO_2, and the

133    $ClNO_2$ was synthesized by the uptake of a known concentration of N_2O_5 on a NaCl slurry (see

134   Wang T et al., 2016 and Tham et al., 2016 for details). The average sensitivity of N_2O_5 and

135    $ClNO_2$ was 0.9 ± 0.3 and 0.7 ± 0.2 Hz pptv^{-1}, respectively. The dependence of the sensitivity

136   on the relative humidity was measured during the field study (see Fig. S1) which was used to

137   correct for the RH effect based on the measured ambient RH values. The detection limits of

138   N_2O_5 and $ClNO_2$ were both 6 pptv (2 σ, 1 min-averaged data).

139   The inlet of the CIMS instrument was set approximately 1.5 m above the roof with 6 m long

140   PFA-Teflon tubing as the sampling line. The total sampling flow was set as 11 standard liters

141   per minute (SLPM). Four SLPM were diverted into the CIMS, O_3 and NO_x analyzer, and the

142   remaining part was evacuated directly from the system. The total residence time was less than

143 1 s in the sampling system. Following our previous practice, the inlet tubing and fittings were

144 replaced every afternoon and washed with an ultrasonic bath to reduce the influence of the

145 tubing wall adhered with deposited particles. The loss of N_2O_5 on the tubing wall was checked

146 on site by injecting N_2O_5 into the ambient air before and after the tubing replacement, and the

147 loss was around 10% in the "clean" tubing and increased to nearly 40% in the next afternoon.

148 Because our analysis mainly focused on data in the first few hours of evening, the loss was

149 insignificant and thus was not corrected in our final data. However, this bias can be important

150 at later period before tube replacement. The uncertainty of the measurement was estimated to

151 be ± 25 % for both N_2O_5 and $ClNO_2$ (Wang T et al., 2016). The time resolution for the

152 measurement was approximately 10 s, and the derived data were later averaged to a time

153 resolution of 1 min for further analysis.

154 **2.3 Other measurements**

155 Trace gases of CO, SO_2, O_3, NO_x, total reactive nitrogen (NO_y), nitrous acid (HONO), C2 to

156 C10 non-methane hydrocarbons (NMHCs), oxygenated hydrocarbons (OVOCs), and aerosol

157 chemical composition and number concentrations were also measured. Table 1 summarized

158 the principle, detection limit and uncertainty of the measuring instruments.

159 CO was observed using a gas filter correlation analyzer (Thermo Model 48i). SO_2 was

160 measured using a pulsed fluorescence analyzer (Thermo Model 43i). O_3 was determined using

161 a UV photometric analyzer (Thermo, Model 49i). NO and NO_2 were detected with a

162 chemiluminescence instrument (Thermo, Model 42i) with a photolytic converter to convert

163 NO_2 to NO (Xu et al., 2013). NO_y was determined using a chemiluminescence analyzer which

164 was equipped with a molybdenum oxide (MoO) catalytic converter (Thermo, Model 42i-Y).

165 HONO was detected using a long path absorption photometer (QUMA, Model LOPAP-03)

166 (Xu et al., 2015). NMHCs were determined using an online gas chromatograph (GC) coupled

167 with a flame ionization detector (FID) and a mass spectrometer (MS) (Wang et al., 2014).

168 NMHCs were only measured from Jan 2 to Jan 8, 2017 due to the maintenance of the GCMS

169 after Jan 8. OVOCs (e.g., formaldehyde, acetaldehyde, acetone, methyl ethyl ketone) were

170 sampled with 2,4-dinitrophenylhydrazine (DNPH) cartridges every 3 h and were later

171 analyzed with a high-performance liquid chromatography (HPLC) system (Cui et al., 2016).

172 Concentrations of $PM_{2.5}$ were detected with a multi-angle absorption photometer (MAAP,

173 Thermo Model 5012). The ionic compositions of $PM_{2.5}$ were measured with an ion

174 chromatography (GAC-IC) system equipped with a gas and aerosol collector at a time

175 resolution of 30 min (Dong et al., 2012) , and the data were also averaged every 1 h to meet

176 the time resolution of other components of $PM_{2.5}$. Organic carbon (OC) and elemental carbon

177 (EC) were measured with an online OC/EC analyzer (RT-4, SUNSET) with a time resolution

178 of 1 h (Bauer et al., 2009). A scanning mobility particle sizer (SMPS Model 3936L75, TSI)

179 was used to determine the dry-state particle number size distribution, covering the size range

180 from 16.5 to 1000 nm. The ambient (wet) particle number size distributions were estimated

181 based on a size-resolved kappa-Köhler function considering the variation with the relative

182 humidity (Hennig et al., 2005; Liu et al., 2014). In the present study, data with RH greater

183 than 90% were excluded because large uncertainty of the growth factor at very high RH. The

184 aerosol surface area density was then derived using the ambient particle number size

185 distribution (wet) and an assumption of spherical particles with an estimated uncertainty of

186 around 30% (Tham et al., 2016; Wang Z et al., 2017).

187 Meteorological parameters were measured with a portable weather station (Model WXT520,

188 Vaisala, Finland), including temperature, relative humidity (RH), wind direction, wind speed,

189 and pressure. A pyranometer (CMP22, Kipp & Zonen B.V., Holland) was used to measure the

190 solar radiation and the data were then utilized to derive the photolysis frequency of NO_2 based

191 on the method of Trebs et al. (2009).

192 **2.4 Chemical box model**

193 To estimate the daytime formation of nitric acid via the reaction of $OH + NO_2$, an

194 observation-based chemical box model developed with the latest version of the Master

195 Chemical Mechanism v3.3.1 (Jenkin et al., 2003; Jenkin et al., 2015; Saunders et al., 2003)

196 and an updated chlorine (Cl) radical chemistry module (Xue et al., 2015) was utilized to

197 estimate the mixing ratio of OH radicals and the reaction rate of $OH + NO_2$. The integrated

198 production of nitric acid during the daytime was then calculated based on the simulation

199 results. The box model was constrained with the observation data every 10 min, including the

200 data of N_2O_5, $ClNO_2$, HONO, O_3, NO, NO_2, SO_2, CO, C2 to C10 NMHCs, OVOCs

201   (formaldehyde, acetaldehyde, acetone, and MEK), temperature, aerosol surface area density

202   and $J(NO_2)$, which were first averaged or interpolated. Average concentrations of NMHC

203   species during the daytime (7:00 to 17:00) and nighttime (17:00 to 7:00 of the next day) are

204   shown in Table S1. A function considering the variation of the solar zenith angle (Saunders et

205   al., 2003) was used to calculate the photolysis frequencies of HONO, O_3 and other species in

206   clear sky, which were then corrected with the $J(NO_2)$ values in the real environment. The

207     $J(ClNO_2)$ was treated the same as in Tham et al. (2016). The lifetime of unconstrained species

208   respect to the physical loss was set as 8 h in a boundary layer of 1000 m depth (equivalent to

209   3.47×10^{-5} s^{-1}) in order to avoid their accumulation. The model was run from 0:00 of Jan 3 to

210   11:00 of Jan 8, 2017. To stabilize the intermediate species, the simulation for the first 24 h

211   was repeated six times. Sensitivity tests were carried out by reducing the input concentrations

212   by 10% to check the deviation of the average daytime (7:00-17:00) rate of OH+NO_2 reaction.

213   The simulated rate of OH+NO_2 reaction was most sensitive to HONO, followed by NO_x and

214   OVOCs (see Text S1 and Fig. S2).

215   **3 Results and discussion**

216   **3.1 Overview of the observation**

217   Figure 2 shows the time series of N_2O_5, $ClNO_2$, components of $PM_{2.5}$, related trace gases and

218   meteorological parameters from 18:40 of Jan 2 to 11:00 of Jan 15, 2017. The average

219   temperature and RH during the measurement period were 17 ± 4℃ and 86 ± 14%,

220   respectively. A severe pollution episode occurred on Jan 3 to 7 due to stagnant meteorological

221   conditions (Fig. 3 (a)), and the concentrations of most pollutants decreased to very low levels

222   on Jan 9 and Jan 12 to 15, which corresponded to the change in weather conditions. The most

223   polluted days were Jan 5 and 6 with the highest $PM_{2.5}$ of 400 μg m^{-3} and the highest O_3 of 160

224   ppbv. The $PM_{2.5}$ data from the PRD regional air quality monitoring network revealed that the

225   HGS site was within the most polluted area during this haze event (Fig. 3(b)). This pollution

226   event was characterized by concurrent high levels of $PM_{2.5}$ and O_3 and was in contrast to the

227   winter haze in north China, which experienced high $PM_{2.5}$ but low O_3 (e.g., Sun et al., 2016;

228   Wang H et al., 2018a). The mixing ratios of N_2O_5 and $ClNO_2$ were up to 3358 pptv and 8324

229   pptv (1 min time resolution), respectively, indicating active N_2O_5 heterogeneous chemistry.

230   Very high concentrations of aerosol nitrate (up to 108 μg m^{-3}, 1 h time resolution) were also

231   observed during the multi-day episode. Nitrate contributed to 24% of the total PM$_{2.5}$ mass

232   concentration on average, which was comparable to that of organic matter (OM = 1.7*OC,

233   28%) and much higher than that of sulfate (16%) and ammonium (11%). The contribution of

234   nitrate to the PM$_{2.5}$ increased with an increase in nitrate concentration, and reached nearly 40%

235   at its highest nitrate level, indicating that nitrate was a dominant component of the PM$_{2.5}$ on

236   the most polluted days. The concentration of NO$_3^-$ exhibited a concurrent increase with that of

237   ClNO$_2$ in the early nighttime on Jan 3 to 4, Jan 4 to 5, Jan 5 to 6 and Jan 9 to 10 (see Fig. 4),

238   suggesting that N$_2$O$_5$ heterogeneous reactions significantly contributed to the formation of

239   nitrate during the nighttime. The measured increases of the NO$_3^-$ concentration during these

240   four nights were 17.1, 50.9, 43.3 and 32.7 μg m^{-3}, respectively. A similar increase in ClNO$_2$

241   was observed on Jan 6 to 7, but the composition of the PM$_{2.5}$ was not available due to

242   instrument maintenance. Apart from chemical reactions, the evolution of the Planetary

243   Boundary Layer (PBL) also affects the concentrations of trace gas and aerosols. The height of

244   PBL generally decreases after sunset with the faster drop in temperature of land, which could

245   lead to the accumulation of primary pollutants (and secondary pollutants) at surface if

246   significant local sources are present. For example, on the night Jan 4-5 (see Fig. 5), the CO

247   and NO$_y$ levels increased between 18:00-19:00 with enhancement of ClNO$_2$ and nitrate,

248   indicative of accumulation of primary emissions, but afterward the primary pollutants

249   decreased for three hours while the latter two continued to increase due to the nighttime

250   chemical process.

251   In the remainder of this manuscript, we will focus on the detailed analysis of

252   above-mentioned five nights to investigate the role of N$_2$O$_5$ heterogeneous chemistry in

253   nitrate formation.

254   **3.2 N$_2$O$_5$ heterogeneous chemistry on the selected nights**

255   **3.2.1 Production of NO$_3$ and N$_2$O$_5$**

256   The first step in the nighttime nitrate formation via N$_2$O$_5$ chemistry is the production of NO$_3$

257   and N$_2$O$_5$. To get insight into the key factors affecting the NO$_3$/N$_2$O$_5$ chemistry, the variation

258   of N_2O_5 and production rate of NO_3 were examined with some relevant gases and

259   meteorological parameters of the five nights. Fig. 5 shows the data of the night of Jan 4 to 5

260   as an example. Some common features were identified for all five nights. In general, low

261   wind speed (< 2.0 m s^{-1}) at night facilitated the accumulation of air pollutants, and high RH

262   was favorable for N_2O_5 heterogeneous uptake. In addition, high aerosol surface area density

263   provided interfaces for N_2O_5 heterogeneous reactions.

264   In the first couple of hours after sunset (Fig 5, red rectangle), N_2O_5 exhibited a peak and

265   quickly dropped to hundreds of pptv, while nitrate and $ClNO_2$ concurrently increased, which

266   was indicative of the local production and loss of N_2O_5. NO was below the detection limit

267   during this period. The production rates of NO_3 ($P_{NO_3}= k_{NO_2+O_3}[NO_2][O_3]$) were the fastest

268   just after sunset and decreased gradually due to reduced O_3 levels. There was a period later in

269   the night (22:00 to 01:00) when fresh emissions of NO were observed, and the production of

270   NO_3 was suppressed due to the titration of O_3 by NO. In the later nighttime, NO was below

271   the detection limit (Fig. 5, blue rectangle). During this period, NO_3 and N_2O_5 were produced

272   at moderate rates, and the very low N_2O_5 concentrations (below the detection limit) suggested

273   a fast loss of N_2O_5 probably leading to the local production of $ClNO_2$ and nitrate, which was

274   not revealed in the observed variations of $ClNO_2$ and nitrate. The concentrations of $ClNO_2$

275   and nitrate during this period fluctuated due to the change in the air masses indicated by the

276   change in SO_2 concentrations and wind speeds.

277   **3.2.2 N_2O_5 uptake coefficient and $ClNO_2$ yield**

278   The N_2O_5 uptake coefficient and $ClNO_2$ yield, together with the reactivity of NO_3 with NO

279   and VOCs, determines the loss pathways of NO_3 and N_2O_5. To derive the uptake coefficient of

280   N_2O_5, a method suggested by McLaren et al. (2010) was applied by treating NO_3 and N_2O_5 as

281   a whole ($[NO_3] + [N_2O_5]$) without assuming the chemical system in the steady state. This

282   approach considers that the change of NO_3 and N_2O_5 concentrations is mainly due to

283   NO_3/N_2O_5 chemistry, and thus it requires that the air mass have relatively stable chemical

284   conditions and not be subject to fresh NO emissions. It also requires that $ClNO_2$ is produced

285   from the N_2O_5 chemistry and has an increasing trend to derive the yield of $ClNO_2$. This

286   method is applicable for the early nighttime (red rectangle, section 3.2.1) for these five nights.

287   The variation rate of $[NO_3] + [N_2O_5]$ can be calculated by deducting the production rate of

288    $[NO_3] + [N_2O_5]$ with its loss rate as Eq. (1).

289   (1) $\frac{d([N_2O_5]+[NO_3])}{dt}=P_{NO_3}-L_{N_2O_5+NO_3}$

290   The loss of $[NO_3] + [N_2O_5]$ is through the NO_3 reaction with VOCs and N_2O_5 heterogeneous

291   reactions, which can both be expressed as pseudo first order losses as Eq. (2):

292   (2) $L_{N_2O_5+NO_3}= L_{NO_3}+ L_{N_2O_5} = k'_{NO_3}[NO_3] + k'_{N_2O_5}[N_2O_5]$

293   where k_{NO3} and k_{N2O5} represent the total first order rate constants for NO_3 and N_2O_5,

294   respectively. The loss rate of N_2O_5 can then be obtained from Eq. (3):

295   (3) $L_{N_2O_5} = k'_{N_2O_5}[N_2O_5]= k_{NO_2+O_3}[NO_2][O_3]-\frac{d[N_2O_5]}{dt}-\frac{d[NO_3]}{dt}-k'_{NO_3}[NO_3]$

296   Because NO_3 was not measured, it was calculated by assuming an equilibrium of

297   NO_2-NO_3-N_2O_5 as shown in Eq. (4). High levels of NO would break this equilibrium. Thus,

298   the periods with detected NO were excluded. $d[NO_3]/dt$ and $d[N_2O_5]/dt$ were calculated as the

299   rate of change of NO_3 and N_2O_5 in a time resolution of 10 min. k_{NO3} was derived with the

300   measured concentrations of NMHCs as Eq. (5) by interpolating the data of NMHCs to 10 min

301   time resolution. The NO_3 reactivity with VOCs (k'_{NO3}) in the early nighttime ranged from

302   0.516 to $1.54\times10^{-3}\,s^{-1}$ (Table 2), which was higher than those derived at Mt. TMS in winter

303   2013 (0.17 to $1.1\times10^{-3}\,s^{-1}$) (Brown et al., 2016), but lower than those in the North China Plain

304   during the summertime (2 to $57\times10^{-3}\,s^{-1}$) (Tham et al., 2016; Wang H et al., 2017, 2018b;

305   Wang Z et al., 2017). NMHCs were not measured on Jan 9 to 10, 2017. We used the average

306   k'_{NO3} in the early nighttime on Jan 3 to 4 as a replacement because these two periods had

307   similar pollution levels for most pollutants. For the later nighttime (Fig. 5, blue rectangle),

308   low levels of N_2O_5 and moderate levels of P_{NO3} also made Eq. (3) inapplicable even though

309   NO was not detected.

310   (4) $[NO_3]= \frac{[N_2O_5]}{[NO_2]\times K_{eq}}$

311   (5) $k'_{NO_3} = \sum k_i[VOC_i]$

312   Finally, the uptake coefficient of N_2O_5 was derived using Eq. (6) for every 10 min and

313   averaged for the whole selected periods. In Eq. (6), C_{N2O5} is the mean molecular speed of

314   N_2O_5, and S_a is the aerosol surface area density. The yield of $ClNO_2$ was derived from Eq. (7)

315   by dividing the integrated production of $ClNO_2$ ($[ClNO_2]_{max}$) to the integrated loss of N_2O_5

316   since sunset.

317   (6) $k'_{N_2O_5} = \frac{L_{N_2O_5}}{[N_2O_5]} = \frac{1}{4} C_{N_2O_5} S_a \gamma_{N_2O_5}$

318   (7) $\phi = \frac{[ClNO_2]_{max}}{\int L_{N_2O_5} dt}$

319   The relative importance of NO_3 reactions with VOCs and N_2O_5 heterogeneous reactions can

320   be examined by comparing the values of the loss coefficient of NO_3 reactions ($\frac{k'_{NO_3}}{[NO_2] \times K_{eq}}$) and

321   N_2O_5 heterogeneous reactions (k'_{N2O5}) (Tham et al., 2016). Based on the calculations, the

322   values of $\frac{k'_{NO_3}}{[NO_2] \times K_{eq}}$ were 1.40×10^{-5} to 6.07×10^{-5} s^{-1} (see Table 2), while that of k'_{N2O5} were

323   3.78×10^{-3} to 9.00×10^{-3} s^{-1}, which was two orders of magnitude higher than that of $\frac{k'_{NO_3}}{[NO_2] \times K_{eq}}$,

324   suggesting that N_2O_5 heterogeneous reactions were the dominant loss pathway of NO_3 and

325   N_2O_5.

326   The average γ_{N2O5} and ϕ_{ClNO2} derived for the early night of the five cases are listed in Table 2.

327   The data show that the uptake coefficient ranged from 0.009 to 0.066, which was comparable

328   to the previous values derived at Mt. Tai Mo Shan (TMS) in Hong Kong (0.004 to 0.022)

329   (Brown et al., 2016) and in the North China Plain (0.006 to 0.102) (Tham et al., 2018; Tham

330   et al., 2016; Wang H et al., 2017, 2018b; Wang X et al., 2017; Wang Z et al., 2017; Zhou et al.,

331   2018). It is interesting to see much higher γ_{N2O5} (0.066) on Jan 3 than those in other four

332   nights (0.009-0.015), resulting from higher P_{NO3} but much lower Sa and relatively low N_2O_5

333   concentrations on Jan 3. We examined known factors affecting the loss of NO_3 and N_2O_5 such

334   as the concentrations of NO, NMHCs and aerosol compositions, but found no obvious

335   difference between Jan 3 and other nights. The yield in this study varied from 0.18 to 0.32,

336   which was similar to most studies in China (Tham et al., 2018; Tham et al., 2016; Wang Z et

337   al., 2017; Yun et al., 2018; Zhou et al., 2018).

3.3 Nitrate formation potential $p(NO_3^-)$ through N_2O_5 chemistry

3.3.1 Nighttime $p(NO_3^-)$

The formation potential of NO_3^- through N_2O_5 chemistry is the total amount of NO_3^-

accumulated from N_2O_5 heterogeneous loss. It can be calculated by deducting the integrated

loss of N_2O_5 with the integrated production of $ClNO_2$ as Eq. (8).

(8) $p(NO_3^-) = (2-\phi) \int L_{N_2O_5} \, dt = 2 \int L_{N_2O_5} \, dt - [ClNO_2]_{max}$

In the early nighttime, the average loss rate of N_2O_5 (L_{N2O5}) ranged from 1.9 to 4.3 ppbv h^{-1}

(Table 2), which was close to the average P_{NO3} due to the dominance of the N_2O_5

heterogeneous reactions in NO_3 and N_2O_5 loss. Based on the derived N_2O_5 loss rate and the

maximum $ClNO_2$ concentration, the formation potential of NO_3^- was derived and ranged from

29.0 to 77.3 μg m^{-3} as shown in Fig. 6. The measured increase of the NO_3^- concentration in the

early nighttime can be completely explained by the integrated production of NO_3^- via the

N_2O_5 heterogeneous reactions during the same period.

In the later nighttime, the method described in section 3.2.2 was not valid for calculating the

N_2O_5 heterogeneous loss rate as mentioned above. We attempted to estimate the formation

potential of nitrate by assuming that the N_2O_5 heterogeneous reactions continued to dominate

the loss of $NO_3 + N_2O_5$ in the later nighttime. The k_{NO3} in the later nighttime were comparable

to those in the early nighttime, and the high RH close to 100% in the later nighttime was

favorable for the N_2O_5 heterogeneous reactions. We assumed that all NO_3 was quickly

consumed by the N_2O_5 heterogeneous reactions, which means that the loss rate of N_2O_5

approximated to the production rate of NO_3 ($L_{N2O5} \approx P_{NO3}$). As listed in Table 3, the N_2O_5 loss

365   rates ranged from 0.82 to 1.26 ppbv h^{-1}, which were significantly lower than those derived in

366   the early nighttime. The derived N_2O_5 loss rate here and the yield of $ClNO_2$ in the early

367   nighttime were used to estimate the formation potential of NO_3^- in the later nighttime. As

368   shown in Fig.6, the nitrate produced during these later periods ranged from 7.3 to 40.3 μg m^{-3},

369   which was lower than those in the early nighttime for four nights, indicating that the nighttime

370   nitrate from N_2O_5 chemistry was mainly produced in the early nighttime.

371   **3.3.2 Comparison with daytime production of HNO_3**

372   During the daytime, the formation of NO_3^- is mainly from the gas-particle partitioning of the

373   gas phase HNO_3 formed through the $OH + NO_2$ reaction. Hence, the daytime formation

374   potential of HNO_3 ($p(HNO_3)$) can be treated as the upper limit for the locally-produced

375   daytime aerosol nitrate. To calculate the daytime $p(HNO_3)$, a box model based on MCM

376   v3.3.1 was used to derive the mixing ratio of OH and the rates of $OH + NO_2$ as described in

377   section 2.4. This model was previously used in our study at Wangdu in North China (Tham et

378   al., 2016). The calculated mixing ratios of OH at Wangdu with this model compared well with

379   those observed by the laser-induced fluorescence (LIF) technique (Tan et al., 2017). In the

380   present study, the average daytime OH (7:00 to 17:00) mixing ratios were 1.71 to $3.82×10^6$

381   molec cm^{-3} during Jan 3 to 7 as listed in Table 4 with the maximum values reaching 3.24 to

382    $6.71×10^6$ molec cm^{-3}. The detailed results for OH can be found in Fig. S3.

383   The average production rates of HNO_3 through the $OH + NO_2$ reaction were 1.40 to 5.21 ppbv

384   h^{-1} from Jan 3 to Jan 7, and the integrated formation potential of HNO_3 during the daytime

385   was 35.7 to 131.8 μg m^{-3}, which was comparable to the nighttime $p(NO_3^-)$ ranging from 69.3

386   to 102.9 μg m^{-3} (Fig. 7). Nighttime production of nitrate via the heterogeneous uptake of N_2O_5

387   accounted for 43.8% to 57.7% of the total nitrate ($NO_3^- + HNO_3$) produced in a 24 h period at

388   the site. These results underscored the important role of N_2O_5 heterogeneous chemistry in

389   nitrate formation in this severe winter haze in southern China.

390   **4 Concluding remarks**

391   With the use of concurrent measurements of nitrate, $ClNO_2$ and related pollutants, this study

392   demonstrates the important contribution of N_2O_5 heterogeneous uptake in nitrate formation.

Current chemical transport models have difficulties in simulating this nitrate production pathway. Therefore, more research efforts are needed to improve the representations of γ_{N2O5} and ϕ_{ClNO2} for better prediction of nitrate in the models. The observation-based approach presented here can be applied to investigate nitrate formation in other areas.

5 Data availability

The data used in this study are available upon request from Tao Wang (cetwang@polyu.edu.hk) and Dingli Yue (dingliyue@163.com).

Author contributions

TW designed the research; WW conducted CIMS measurement; YZ, DY, HY, MX, CY and PS performed the measurements of other parameters used in this study; HY, TW, MX and WW analyzed the data; HY and TW wrote the manuscript. All authors contributed to discussion and commented on the manuscript.

References

Anttila, T., Kiendler-Scharr, A., Tillmann, R., and Mentel, T. F.: On the reactive uptake of gaseous compounds by organic-coated aqueous aerosols: Theoretical analysis and application to the heterogeneous hydrolysis of N_2O_5, The Journal of Physical Chemistry A, 110, 10435-10443, 2006.

Bauer, J. J., Yu, X.-Y., Cary, R., Laulainen, N., and Berkowitz, C.: Characterization of the sunset semi-continuous carbon aerosol analyzer, J Air Waste Manage, 59, 826-833, 2009.

Bertram, T., and Thornton, J.: Toward a general parameterization of N_2O_5 reactivity on aqueous particles: the competing effects of particle liquid water, nitrate and chloride, Atmos Chem Phys, 9, 8351-8363, 2009.

Brown, S. S., and Stutz, J.: Nighttime radical observations and chemistry, Chem Soc Rev, 41,

6405-6447, 2012.

Brown, S. S., Dubé, W. P., Tham, Y. J., Zha, Q., Xue, L., Poon, S., Wang, Z., Blake, D. R., Tsui, W., and Parrish, D. D.: Nighttime Chemistry at a High Altitude Site Above Hong Kong, J. Geophys. Res. Atmos., 121, 2457–2475, doi: 10.1002/2015JD024566, 2016.

Chang, W. L., Bhave, P. V., Brown, S. S., Riemer, N., Stutz, J., and Dabdub, D.: Heterogeneous Atmospheric Chemistry, Ambient Measurements, and Model Calculations of N_2O_5: A Review, Aerosol Sci Tech, 45, 665-695, doi:10.1080/02786826.2010.551672, 2011.

Cui, L., Zhang, Z., Huang, Y., Lee, S. C., Blake, D. R., Ho, K. F., Wang, B., Gao, Y., Wang, X. M., and Louie, P. K. K.: Measuring OVOCs and VOCs by PTR-MS in an urban roadside microenvironment of Hong Kong: relative humidity and temperature dependence, and field intercomparisons, Atmos Meas Tech, 9, 5763-5779, 2016.

Davis, J. M., Bhave, P. V., and Foley, K. M.: Parameterization of N_2O_5 reaction probabilities on the surface of particles containing ammonium, sulfate, and nitrate, Atmos Chem Phys, 8, 5295-5311, 2008.

Dentener, F. J., and Crutzen, P. J.: Reaction of N_2O_5 on tropospheric aerosols: Impact on the global distributions of NO_x, O_3, and OH, J. Geophys. Res. Atmos., 98, 7149-7163, 1993.

Dong, H.B., Zeng, L.M., Hu, M., Wu, Y.S., Zhang, Y.H., Slanina, J., Zheng, M., Wang, Z.F., and Jansen, R.: Technical Note: The application of an improved gas and aerosol collector for ambient air pollutants in China, Atmos. Chem. Phys., 12, 10519-10533, doi:10.5194/acp-12-10519-2012, 2012.

Evans, M. J., and Jacob, D. J.: Impact of new laboratory studies of N_2O_5 hydrolysis on global model budgets of tropospheric nitrogen oxides, ozone, and OH, Geophys. Res. Lett., 32, L09813, doi: 10.1029/2005GL022469, 2005.

Finlayson-Pitts, B. J., Ezell, M. J., and Pitts, J. N.: Formation of chemically active chlorine compounds by reactions of atmospheric NaCl particles with gaseous N_2O_5 and $ClONO_2$, Nature, 337, 241-244, 1989.

Fu, X., Wang, X., Guo, H., Cheung, K., Ding, X., Zhao, X., He, Q., Gao, B., Zhang, Z., and Liu, T.: Trends of ambient fine particles and major chemical components in the Pearl River Delta region: observation at a regional background site in fall and winter, Sci Total Environ, 497, 274-281, 2014.

Ge, X., He, Y., Sun, Y., Xu, J., Wang, J., Shen, Y., and Chen, M.: Characteristics and formation mechanisms of fine particulate nitrate in typical urban areas in China, Atmosphere, 8, 62, 2017.

Geng, G., Zhang, Q., Tong, D., Li, M., Zheng, Y., Wang, S., and He, K.: Chemical composition of ambient PM2. 5 over China and relationship to precursor emissions during 2005-2012, Atmos. Chem. Phys, 17, 9187-9203, 2017.

Hennig, T., Massling, A., Brechtel, F., and Wiedensohler, A.: A tandem DMA for highly temperature-stabilized hygroscopic particle growth measurements between 90% and 98% relative humidity, J Aerosol Sci, 36, 1210-1223, 2005.

Huang, R. J., Zhang, Y. L., Bozzetti, C., Ho, K. F., Cao, J. J., Han, Y. M., Daellenbach, K. R., Slowik, J. G., Platt, S. M., Canonaco, F., Zotter, P., Wolf, R., Pieber, S. M., Bruns, E. A., Crippa, M., Ciarelli, G., Piazzalunga, A., Schwikowski, M., Abbaszade, G., Schnelle-Kreis, J., Zimmermann, R., An, Z. S., Szidat, S., Baltensperger, U., El Haddad, I., and Prevot, A. S. H.: High secondary aerosol contribution to particulate pollution during haze events in China, Nature, 514, 218-222, Doi: 10.1038/Nature13774, 2014.

466 Jenkin, M. E., Saunders, S. M., Wagner, V., and Pilling, M. J.: Protocol for the development of the
467   Master Chemical Mechanism, MCM v3 (Part B): tropospheric degradation of aromatic volatile
468   organic compounds, Atmos Chem Phys, 3, 181-193, 2003.
469 Jenkin, M. E., Young, J. C., and Rickard, A. R.: The MCM v3.3.1 degradation scheme for isoprene,
470   Atmos Chem Phys, 15, 11433-11459, 2015.
471 Li, H., Zhang, Q., Zheng, B., Chen, C., Wu, N., Guo, H., Zhang, Y., Zheng, Y., Li, X., and He, K.:
472   Nitrate-driven urban haze pollution during summertime over the North China Plain, Atmos Chem
473   Phys, 18, 5293-5306, 2018.
474 Li, W., Liu, X., Zhang, Y., Sun, K., Wu, Y., Xue, R., Zeng, L., Qu, Y., and An, J.: Characteristics and
475   formation mechanism of regional haze episodes in the Pearl River Delta of China, Journal of
476   Environmental Sciences, 63,236-249, 2017.
477 Liu, H., Zhao, C., Nekat, B., Ma, N., Wiedensohler, A., Van Pinxteren, D., Spindler, G., Müller, K., and
478   Herrmann, H.: Aerosol hygroscopicity derived from size-segregated chemical composition and its
479   parameterization in the North China Plain, Atmos Chem Phys, 14, 2525-2539, 2014.
480 Liu, X., Sun, K., Qu, Y., Hu, M., Sun, Y., Zhang, F., and Zhang, Y.: Secondary formation of sulfate and
481   nitrate during a haze episode in megacity Beijing, China, Aerosol Air Qual. Res, 15, 2246-2257,
482   2015.
483 Makar, P., Wiebe, H., Staebler, R., Li, S., and Anlauf, K.: Measurement and modeling of particle nitrate
484   formation, J. Geophys. Res. Atmos., 103, 13095-13110, 1998.
485 McDuffie, E. E., Fibiger, D. L., Dubé, W. P., Lopez-Hilfiker, F., Lee, B. H., Thornton, J. A., Shah, V.,
486   Jaeglé, L., Guo, H., and Weber, R. J.: Heterogeneous N_2O_5 uptake during winter: Aircraft
487   measurements during the 2015 WINTER campaign and critical evaluation of current
488   parameterizations, J. Geophys. Res. Atmos., 123, 4345-4372, doi: 10.1002/2018JD028336, 2018.
489 McLaren, R., Wojtal, P., Majonis, D., McCourt, J., Halla, J. D., and Brook, J.: NO_3 radical
490   measurements in a polluted marine environment: links to ozone formation, Atmos. Chem. Phys.,
491   10, 4187-4206, 2010.
492 Munger, J. W., Fan, S. M., Bakwin, P. S., Goulden, M. L., Goldstein, A., Colman, A. S., and Wofsy, S.
493   C.: Regional budgets for nitrogen oxides from continental sources: Variations of rates for
494   oxidation and deposition with season and distance from source regions, J. Geophys. Res. Atmos.,
495   103, 8355-8368, 1998.
496 Pathak, R. K., Wu, W. S., and Wang, T.: Summertime $PM_{2.5}$ ionic species in four major cities of China:
497   Nitrate formation in an ammonia-deficient atmosphere, Atmos Chem Phys, 9, 1711-1722, 2009.
498 Pathak, R. K., Wang, T., and Wu, W. S.: Nighttime enhancement of $PM_{2.5}$ nitrate in ammonia-poor
499   atmospheric conditions in Beijing and Shanghai: Plausible contributions of heterogeneous
500   hydrolysis of N_2O_5 and HNO_3 partitioning, Atmos Environ, 45, 1183-1191,
501   doi:10.1016/j.atmosenv.2010.09.003, 2011.
502 Phillips, G. J., Thieser, J., Tang, M., Sobanski, N., Schuster, G., Fachinger, J., Drewnick, F., Borrmann,
503   S., Bingemer, H., and Lelieveld, J.: Estimating N_2O_5 uptake coefficients using ambient
504   measurements of NO_3, N_2O_5, $ClNO_2$ and particle-phase nitrate, Atmos Chem Phys, 16,
505   13231-13249, 2016.
506 Qu, Z., Henze, D. K., Capps, S. L., Wang, Y., Xu, X., Wang, J., and Keller, M.: Monthly top-down NO_x
507   emissions for China (2005–2012): A hybrid inversion method and trend analysis, J. Geophys. Res.
508   Atmos., 122, 4600-4625, 2017.
509 Reuter, M., Buchwitz, M., Hilboll, A., Richter, A., Schneising, O., Hilker, M., Heymann, J.,

510   Bovensmann, H., and Burrows, J.: Decreasing emissions of NO_x relative to CO_2 in East Asia
511   inferred from satellite observations, Nat Geosci, 7, 792, 2014.

512 Riemer, N., Vogel, H., Vogel, B., Schell, B., Ackermann, I., Kessler, C., and Hass, H.: Impact of the
513   heterogeneous hydrolysis of N_2O_5 on chemistry and nitrate aerosol formation in the lower
514   troposphere under photosmog conditions, J. Geophys. Res., 108, 4144, doi:
515   10.1029/2002JD002436, D4, 2003.

516 Riemer, N., Vogel, H., Vogel, B., Anttila, T., Kiendler‐Scharr, A., and Mentel, T.: Relative importance
517   of organic coatings for the heterogeneous hydrolysis of N_2O_5 during summer in Europe, J.
518   Geophys. Res., 114, D17307, doi: 10.1029/2008JD011369, 2009.

519 Roberts, J. M., Osthoff, H. D., Brown, S. S., Ravishankara, A., Coffman, D., Quinn, P., and Bates, T.:
520   Laboratory studies of products of N_2O_5 uptake on Cl-containing substrates, Geophys. Res. Lett.,
521   36, L20808, doi: 10.1029/2009GL040448, 2009.

522 Saunders, S. M., Jenkin, M. E., Derwent, R. G., and Pilling, M. J.: Protocol for the development of the
523   Master Chemical Mechanism, MCM v3 (Part A): tropospheric degradation of non-aromatic
524   volatile organic compounds, Atmos Chem Phys, 3, 161-180, 2003.

525 Schaap, M., Loon, M. v., Ten Brink, H., Dentener, F., and Builtjes, P.: Secondary inorganic aerosol
526   simulations for Europe with special attention to nitrate, Atmos Chem Phys, 4, 857-874, 2004.

527 Seinfeld, J. H., and Pandis, S. N.: Atmospheric chemistry and physics: from air pollution to climate
528   change, John Wiley & Sons, 2016.

529 Sun, Y., Chen, C., Zhang, Y., Xu, W., Zhou, L., Cheng, X., Zheng, H., Ji, D., Li, J., and Tang, X.: Rapid
530   formation and evolution of an extreme haze episode in Northern China during winter 2015,
531   Scientific reports, 6, 27151, 2016.

532 Tan, Z., Fuchs, H., Lu, K., Hofzumahaus, A., Bohn, B., Broch, S., Dong, H., Gomm, S., Häseler, R., He,
533   L., Holland, F., Li, X., Liu, Y., Lu, S., Rohrer, F., Shao, M., Wang, B., Wang, M., Wu, Y., Zeng, L.,
534   Zhang, Y., Wahner, A., and Zhang, Y.: Radical chemistry at a rural site (Wangdu) in the North
535   China Plain: observation and model calculations of OH, HO_2 and RO_2 radicals, Atmos. Chem.
536   Phys., 17, 663-690, 10.5194/acp-17-663-2017, 2017.

537 Tham, Y. J., Wang, Z., Li, Q., Yun, H., Wang, W., Wang, X., Xue, L., Lu, K., Ma, N., Bohn, B., Li, X.,
538   Kecorius, S., Größ, J., Shao, M., Wiedensohler, A., Zhang, Y., and Wang, T.: Significant
539   concentrations of nitryl chloride sustained in the morning: investigations of the causes and impacts
540   on ozone production in a polluted region of northern China, Atmos. Chem. Phys., 16,
541   14959-14977, doi:10.5194/acp-16-14959-2016, 2016.

542 Tham, Y. J., Wang, Z., Li, Q., Wang, W., Wang, X., Lu, K., Ma, N., Yan, C., Kecorius, S., Wiedensohler,
543   A., Zhang, Y., and Wang, T.: Heterogeneous N_2O_5 uptake coefficient and production yield of
544   ClNO2 in polluted northern China: Roles of aerosol water content and chemical composition,
545   Atmos. Chem. Phys. Discuss., doi:10.5194/acp-2018-313, 2018.

546 Trebs, I., Bohn, B., Ammann, C., Rummel, U., Blumthaler, M., Königstedt, R., Meixner, F., Fan, S.,
547   and Andreae, M.: Relationship between the NO_2 photolysis frequency and the solar global
548   irradiance, Atmos Meas Tech, 2, 725-739, 2009.

549 Wang, H., Lu, K., Chen, X., Zhu, Q., Chen, Q., Guo, S., Jiang, M., Li, X., Shang, D., Tan, Z., Wu, Y.,
550   Wu, Z., Zou, Q., Zheng, Y., Zeng, L., Zhu, T., Hu, M., and Zhang, Y.: High N_2O_5 Concentrations
551   Observed in Urban Beijing: Implications of a Large Nitrate Formation Pathway, Environmental
552   Science & Technology Letters, doi:10.1021/acs.estlett.7b00341, 2017.

553 Wang, H., Lu, K., Chen, X., Zhu, Q., Wu, Z., Wu, Y., and Sun, K.: Large particulate nitrate formation

554   from N_2O_5 uptake in a chemically reactive layer aloft during winter time in Beijing, Atmos. Chem.
555   Phys. Discuss., doi:10.5194/acp-2017-1217, 2018a.

556   Wang, H., Lu, K., Guo, S., Wu, Z., Shang, D., Tan, Z., Wang, Y., Le Breton, M., Zhu, W., Lou, S., Tang,
557   M., Wu, Y., Zheng, J., Zeng, L., Hallquist, M., Hu, M., and Zhang, Y.: Efficient N_2O_5 Uptake and
558   NO_3 Oxidation in the Outflow of Urban Beijing, Atmos. Chem. Phys. Discuss.,
559   doi:10.5194/acp-2018-88, 2018b.

560   Wang, M., Zeng, L., Lu, S., Shao, M., Liu, X., Yu, X., Chen, W., Yuan, B., Zhang, Q., Hu, M., and
561   Zhang, Z.: Development and validation of a cryogen-free automatic gas chromatograph system
562   (GC-MS/FID) for online measurements of volatile organic compounds, Anal. Methods, 6,
563   9424–9434, doi:10.1039/C4AY01855A, 2014.

564   Wang, T., Tham, Y. J., Xue, L., Li, Q., Zha, Q., Wang, Z., Poon, S. C., Dubé, W. P., Blake, D. R., and
565   Louie, P. K.: Observations of nitryl chloride and modeling its source and effect on ozone in the
566   planetary boundary layer of southern China, J. Geophys. Res. Atmos., 121, 2476–2489, doi:
567   10.1002/2015JD024556, 2016.

568   Wang, X., Zhang, Y., Chen, H., Yang, X., Chen, J., and Geng, F.: Particulate nitrate formation in a
569   highly polluted urban area: a case study by single-particle mass spectrometry in Shanghai, Environ
570   Sci Technol, 43, 3061-3066, 2009.

571   Wang, X., Chen, W., Chen, D., Wu, Z., and Fan, Q.: Long-term trends of fine particulate matter and
572   chemical composition in the Pearl River Delta Economic Zone (PRDEZ), China, Frontiers of
573   Environmental Science & Engineering, 10, 53-62, 2016.

574   Wang, X., Wang, H., Xue, L., Wang, T., Wang, L., Gu, R., Wang, W., Tham, Y. J., Wang, Z., Yang, L.,
575   Chen, J., and Wang, W.: Observations of N_2O_5 and $ClNO_2$ at a polluted urban surface site in North
576   China: High N_2O_5 uptake coefficients and low $ClNO_2$ product yields, Atmos Environ, 156,
577   125-134, 2017.

578   Wang, Z., Wang, W., Tham, Y. J., Li, Q., Wang, H., Wen, L., Wang, X., and Wang, T.: Fast
579   heterogeneous N_2O_5 uptake and $ClNO_2$ production in power plant and industrial plumes observed
580   in the nocturnal residual layer over the North China Plain, Atmos. Chem. Phys., 17, 12361-12378,
581   doi:10.5194/acp-17-12361-2017, 2017.

582   Wen, L., Chen, J., Yang, L., Wang, X., Xu, C., Sui, X., Yao, L., Zhu, Y., Zhang, J., and Zhu, T.:
583   Enhanced formation of fine particulate nitrate at a rural site on the North China Plain in summer:
584   The important roles of ammonia and ozone, Atmos Environ, 101, 294-302, 2015.

585   Wen, L., Xue, L., Wang, X., Xu, C., Chen, T., Yang, L., Wang, T., and Wang, W.: Summertime fine
586   particulate nitrate pollution in the North China Plain: Increasing trends, formation mechanisms,
587   and implications for control policy, Atmos. Chem. Phys. Discuss., 2018, 1-27,
588   doi:10.5194/acp-2018-89, 2018.

589   Xu, Z., Wang, T., Xue, L. K., Louie, P. K. K., Luk, C. W. Y., Gao, J., Wang, S. L., Chai, F. H., and
590   Wang, W. X.: Evaluating the uncertainties of thermal catalytic conversion in measuring
591   atmospheric nitrogen dioxide at four differently polluted sites in China, Atmos Environ, 76,
592   221-226, 2013.

593   Xu, Z., Wang, T., Wu, J., Xue, L., Chan, J., Zha, Q., Zhou, S., Louie, P. K. K., and Luk, C. W. Y.:
594   Nitrous acid (HONO) in a polluted subtropical atmosphere: Seasonal variability, direct vehicle
595   emissions and heterogeneous production at ground surface, Atmos Environ, 106, 100-109, 2015.

596   Xue, J., Yuan, Z., Lau, A. K., and Yu, J. Z.: Insights into factors affecting nitrate in $PM_{2.5}$ in a polluted
597   high NOx environment through hourly observations and size distribution measurements, J.

598   Geophys. Res. Atmos., 119, 4888-4902, 2014.

599 Xue, L. K., Saunders, S. M., Wang, T., Gao, R., Wang, X. F., Zhang, Q. Z., and Wang, W. X.:
600   Development of a chlorine chemistry module for the Master Chemical Mechanism, Geoscientific
601   Model Development, 8, 3151-3162, 2015.

602 Yang, T., Sun, Y., Zhang, W., Wang, Z., Liu, X., Fu, P., and Wang, X.: Evolutionary processes and
603   sources of high-nitrate haze episodes over Beijing, Spring, Journal of Environmental Sciences, 54,
604   142-151, 2017.

605 Yue, D., Zhong, L., Zhang, T., Shen, J., Zhou, Y., Zeng, L., Dong, H., and Ye, S.: Pollution properties of
606   water-soluble secondary inorganic ions in atmospheric $PM_{2.5}$ in the Pearl River Delta region,
607   Aerosol Air Qual. Res, 15, 1737-1747, 2015.

608 Yun, H., Wang, T., Wang, W., Tham, Y. J., Li, Q., Wang, Z., and Poon, S. C. N.: Nighttime NO_x loss and
609     $ClNO_2$ formation in the residual layer of a polluted region: Insights from field measurements and
610   an iterative box model, Sci Total Environ, 622-623, 727-734, 2018.

611 Zhang, R., Wang, G., Guo, S., Zamora, M. L., Ying, Q., Lin, Y., Wang, W., Hu, M., and Wang, Y.:
612   Formation of Urban Fine Particulate Matter, Chemical Reviews, 115, 3803-3855, doi:
613   10.1021/acs.chemrev.5b00067, 2015.

614 Zhou, W., Zhao, J., Ouyang, B., Mehra, A., Xu, W., Wang, Y., Bannan, T. J., Worrall, S. D., Priestley,
615   M., Bacak, A., Chen, Q., Xie, C., Wang, Q., Wang, J., Du, W., Zhang, Y., Ge, X., Ye, P., Lee, J. D.,
616   Fu, P., Wang, Z., Worsnop, D., Jones, R., Percival, C. J., Coe, H., and Sun, Y.: Production of N_2O_5
617   and $ClNO_2$ in summer in urban Beijing, China, Atmos. Chem. Phys. Discuss.,
618   doi:10.5194/acp-2018-349, 2018.

619

620

621

622

623

624

625

626

627

628

629

630

Table 1. Technique, limit of detection, and uncertainty of measuring instruments for trace gases and aerosols.

Species	Measurement techniques	Uncertainty	Detection limits
$ClNO_2$, N_2O_5	CIMS	±25%	6 pptv
HONO	LOPAP	±20%	7 pptv
O_3	UV photometry	±5%	0.5 ppbv
NO	Chemiluminescence	±20%	0.06 ppbv
NO_2	Photolytical converter & Chemiluminescence	±20%	0.3 ppbv
NO_y	MoO catalytic converter & Chemiluminescence	±5%	<0.1 ppbv
SO_2	Pulsed-UV fluorescence	±5%	0.1 ppbv
CO	IR photometry	±5%	4 ppbv
NMHCs	GC-FID/MS	±15-20%	20-300 pptv
OVOCs	DNPH-HPLC	±1-15%	20-450 pptv
$PM_{2.5}$	MAAP	±10%	<0.1 $\mu g\ m^{-3}$
Aerosol Ions	GAC-IC	±10%	0.01-0.16 $\mu g\ m^{-3}$
OC/EC	RT-4 SUNSET	± 4-6%	0.2 $\mu g\ cm^{-2}$

Table 2. Average values of N_2O_5 concentrations, N_2O_5 uptake coefficients, $ClNO_2$ yields and other related parameters and maximum values of $ClNO_2$ concentrations in the early nighttime for five selected nights.

Date	N_2O_5 pptv	Max-$ClNO_2$ pptv	NO_2 ppbv	O_3 ppbv	RH %	Sa $\mu m^2\ cm^{-3}$	P_{NO3} ppbv h^{-1}	k'_{NO3} $10^{-3}\ s^{-1}$	L_{N2O5} ppbv h^{-1}	$k'_{NO3}/(Keq[NO_2])$ $10^{-5}\ s^{-1}$	k'_{N2O5} $10^{-3}\ s^{-1}$	γ_{N2O5}	ϕ_{ClNO2}
Jan.3 17:40-19:00	200	1029	20	78	59	2170	4.3	0.516	4.3	3.03	8.81	0.066	0.18
Jan 4 17:00-22:00	700	4608	24	61	82	6452	3.3	1.54	3.2	6.07	4.16	0.009	0.32
Jan 5 17:00-22:00	338	4828	18	73	81	8399	3.4	0.790	3.3	4.06	9.00	0.015	0.29
Jan 6 17:00-22:40	326	2908	13	82	77	5092	2.8	0.677	2.6	4.95	3.78	0.013	0.20
Jan 9 19:00-00:20	121	2553	19	41	85	5173	1.9	0.516	1.9	1.40	4.28	0.015	0.28

642   Table 3. Average values of N_2O_5 loss rate and related parameters for selected periods in the

643   later nighttime.

Date		NO_2 ppbv	O_3 ppbv	P_{NO3} ppbv h^{-1}	k'$_{NO3}$ 10^{-3} s^{-1}	L_{N2O5} ppbv h^{-1}
Jan 3-4	21:00-05:00	20.8	20.7	1.00	0.684	1.00
Jan 5	01:30-06:50	22.4	19.5	0.96	1.45	0.96
Jan 5-6	23:40-01:10	21.1	25.5	1.26	1.13	1.26
Jan 6-7	23:00-06:00	22.1	14.4	0.82	0.709	0.82
Jan 10	01:50-03:30	24.8	15.6	0.90	/	0.90

644

645   Table 4. Average OH mixing ratio and rate of OH + NO_2 during the daytime (7:00 to 17:00 LT)

646   from Jan 3 to Jan 7, 2017.

Date	OH (molec cm^{-3})	NO_2 (ppbv)	OH + NO_2 (ppbv h^{-1})
Jan 3	2.18×10^6	36.2	3.49
Jan 4	2.47×10^6	23.6	2.60
Jan 5	2.62×10^6	30.8	3.09
Jan 6	3.82×10^6	31.5	5.21
Jan 7	1.71×10^6	18.4	1.40

647

648

649

650

651

652

653

654

655

656

657

658
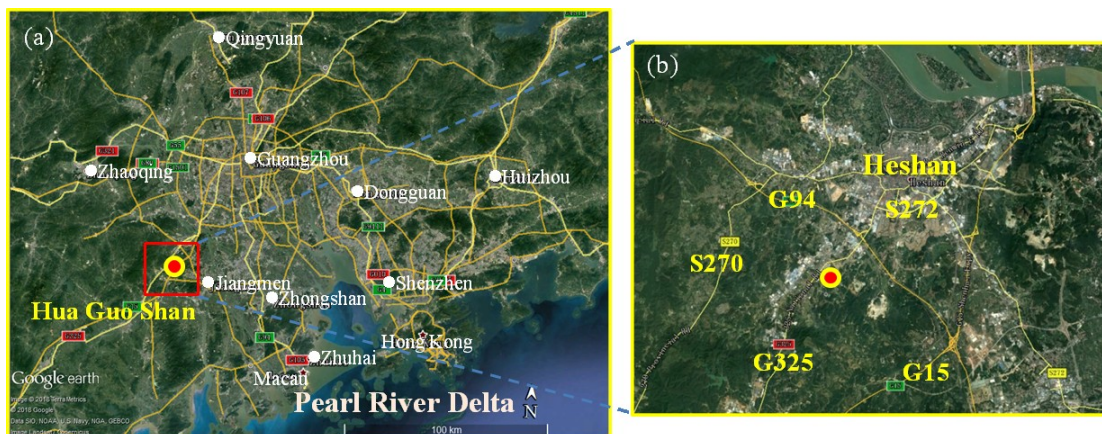
Figure 1. (a) Google map images of the Pearl River Delta in the Guangdong Province and measurement site (Hua Guo Shan). (b) The topography and major roads (shown by number) adjacent to the measurement site.


662
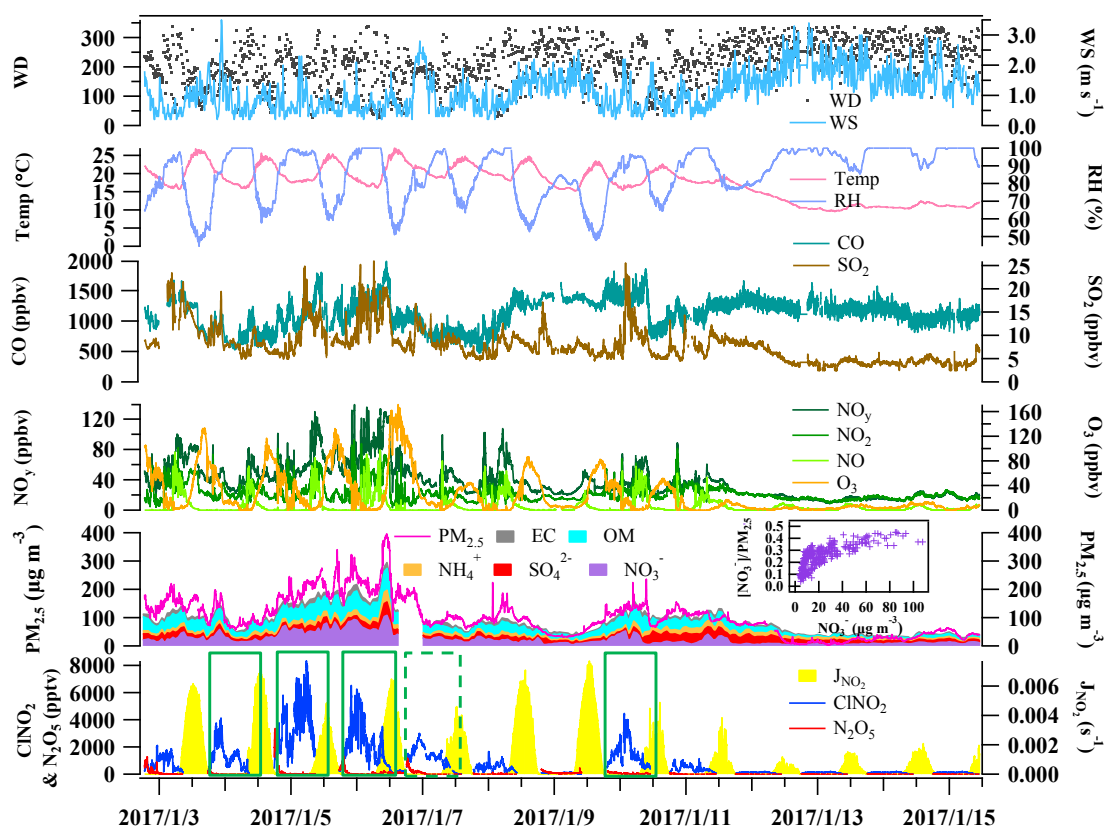
Figure 2. Time series of N_2O_5, $ClNO_2$, components of $PM_{2.5}$, related trace gases and meteorological parameters from 18:40 of Jan 2 to 11:00 of Jan 15, 2017. The inserted figure shows the variation of the ratio of nitrate to $PM_{2.5}$ with increasing nitrate concentration. The green rectangles in the figure indicate the five days used for detailed analysis.

667
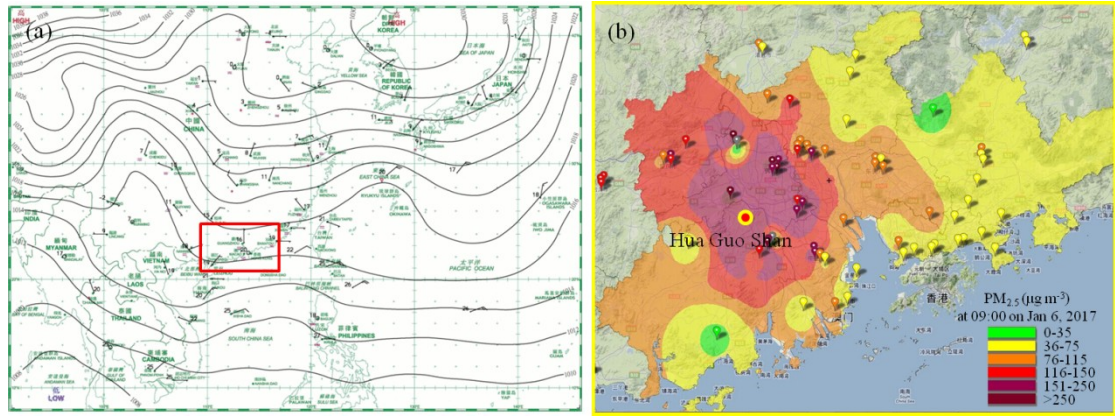
Figure 3. (a) Surface weather chart at 08:00 LT on Jan 6, 2017 downloaded from the website of the Hong Kong Observatory indicating stagnant conditions. (b) The distribution of $PM_{2.5}$ concentrations in the PRD region at 09:00 LT on Jan 6, 2017. This figure was captured from the website. http://113.108.142.147:20031/GDPublish/publish.aspx.
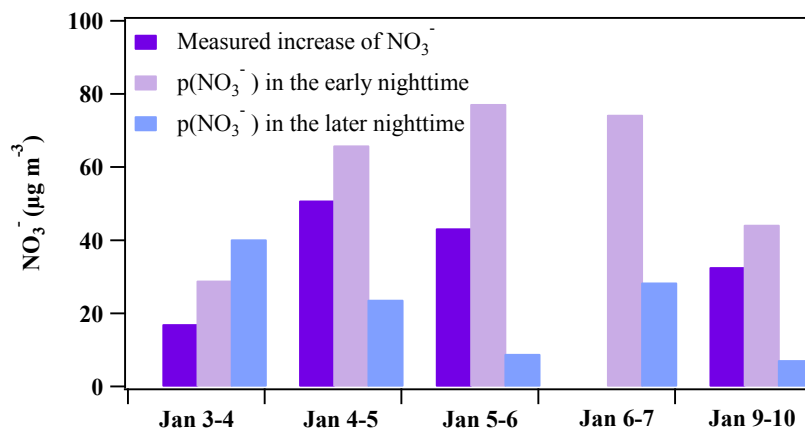

672
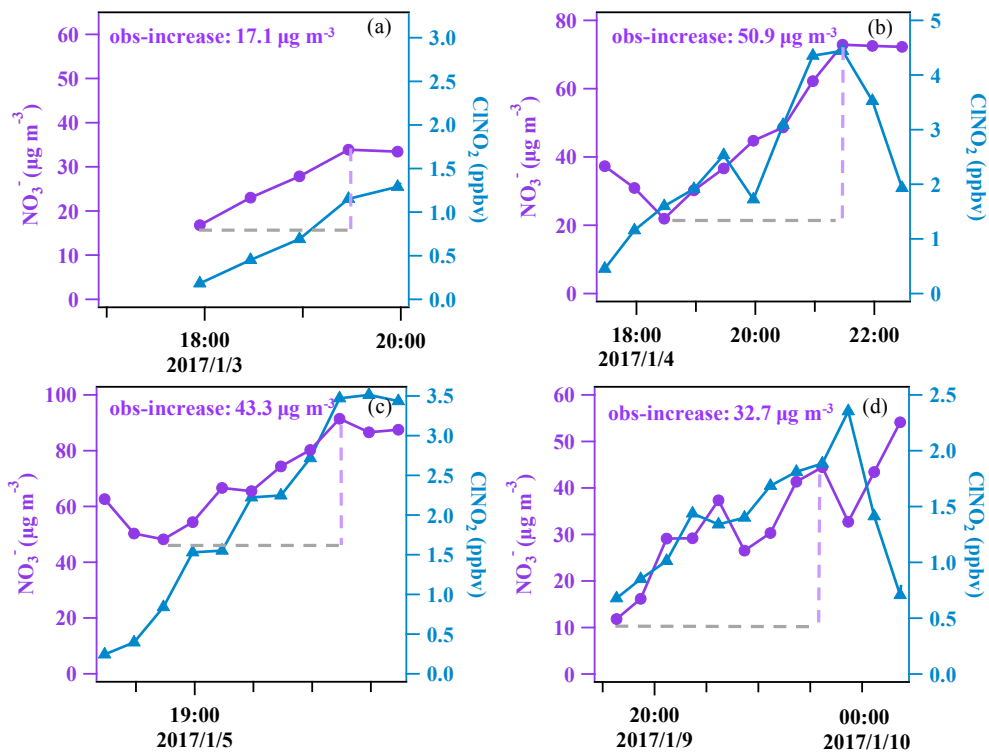
Figure 4. The covariance of aerosol nitrate and $ClNO_2$ in the early nighttime (in 30 min time resolution) for four nights.
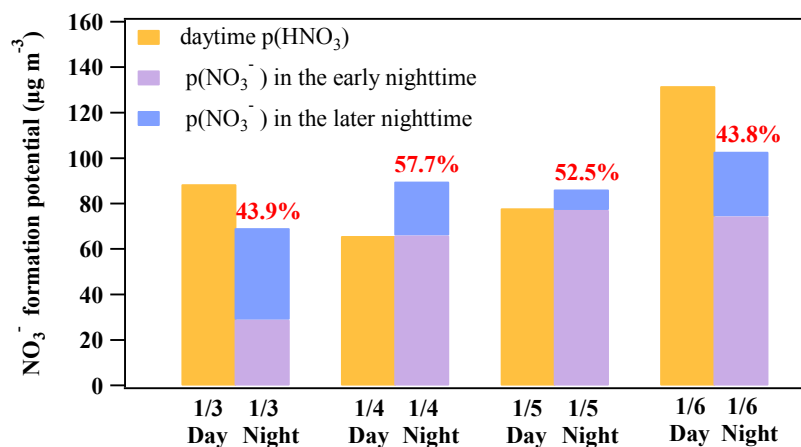
675
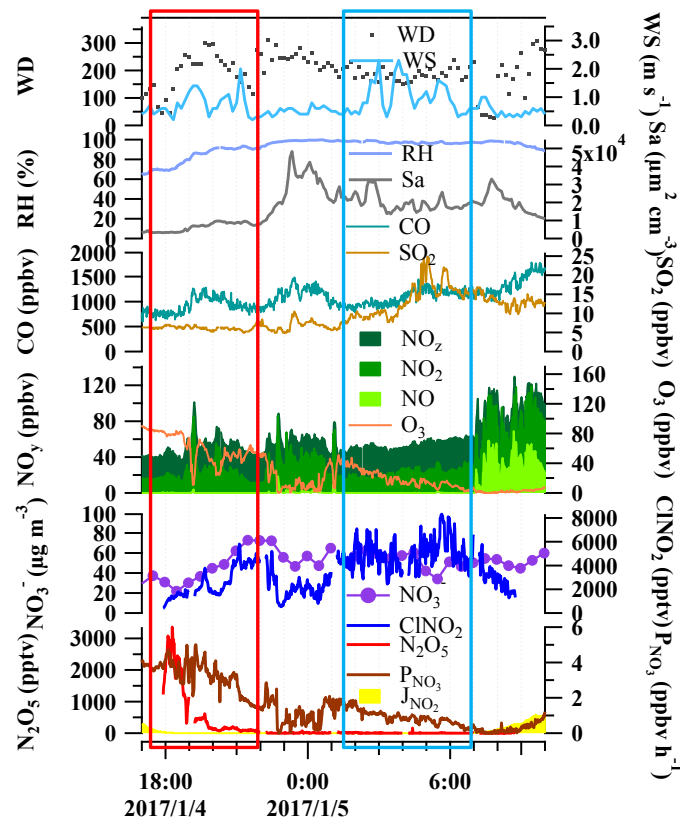
Figure 5. Variation of N_2O_5, $ClNO_2$, NO_3^-, trace gases and meteorological conditions during the nighttime of Jan 4 to 5, 2017 as an example for the five selected nights.

678

Figure 6. Comparison between the measured NO_3^- increase and the NO_3^- formation potential in the early nighttime (periods in Table 2: Jan 3 17:40-19:00, Jan 4 17:00-22:00, Jan 5 17:00-22:00, Jan 6 17:00-22:40, Jan 9 19:00-00:20) and in the later nighttime (periods in Table 3: Jan 3-4 21:00-05:00, Jan 5 01:30-06:50, Jan 5-6 23:40-01:10, Jan 6-7 23:00-06:00, Jan 10 01:50-03:30).

684

Figure 7. Comparison between the daytime (7:00 to 17:00 LT, assuming all gas phase HNO$_3$ partitioned into particle phase) and nighttime (17:00 to 7:00 LT of the next day) NO$_3^-$ formation potential. The early nighttime in each day represents the periods in Table 2, including Jan 3 17:40-19:00, Jan 4 17:00-22:00, Jan 5 17:00-22:00, Jan 6 17:00-22:40, and Jan 9 19:00-00:20. The later nighttime in each day represents the periods in Table 3, including Jan 3-4 21:00-05:00, Jan 5 01:30-06:50, Jan 5-6 23:40-01:10, Jan 6-7 23:00-06:00, and Jan 10 01:50-03:30. The intercomparison of the NO$_3^-$ formation potential in the day and night of Jan 9 and 10 was not conducted due to the lack of data of NMHC after Jan 8 which made the model simulation of OH infeasible on the day of Jan 9.

694